Modeling Photoluminescence Decay Dynamics in Nanocrystals

by

Brian Fernandes

A thesis
presented to the University of Waterloo
in fulfillment of the
thesis requirement for the degree of
Master of Mathematics
in
Applied Mathematics

Waterloo, Ontario, Canada, 2016

I hereby declare that I am the sole author of this thesis. This is a true copy of the thesis, including any required final revisions, as accepted by my examiners.

I understand that my thesis may be made electronically available to the public.

Abstract

Photoluminescence resulting from donor-acceptor recombination in gallium oxide nanocrystals was studied at short and long time scales for different nanocrystal sizes. A model for the intensity decay was formulated with two different donor distributions, one with donors uniformly distributed throughout the volume, and the other with donors restricted to the surface of the nanocrystal. These models were fit to experimental data and the effect of an exclusion distance about the acceptor was explored. A model for the spectrum of emitted light was developed using the same two donor distributions. A modification to the Coulomb interaction was derived by taking into account the dielectric mismatch between the nanocrystal and the surrounding medium. A Monte Carlo algorithm was developed for generating an ensemble of nanocrystals and recording the emitted spectrum. This allowed the model to be expanded to include a distribution of crystal sizes and an arbitrary acceptor position.

Acknowledgements

I am very grateful to my Supervisors Zoran Miskovic and Pavle Radovanovic for their excellent guidance and advice over the past two years. I would also like to thank my committee members Sander Rhebergen and Mohammad Kohandel for taking the time to read my thesis and provide constructive feedback.

Table of Contents

List of Tables

List of Figures

List of Acronyms

TCO	Transparent Conducting Oxide
NC	Nanocrystal
LED	Light Emitting Diode
DAP	Donor-Acceptor Pair
PL	Photoluminescence
TCSPC	Time Correlated Single Photon Counting
PDF	Probability Distribution Function
MC	Monte Carlo

Chapter 1

Introduction

1.1 Summary

Recently there have been significant advances in nanostructured materials due to their technological promise and diverse applications in photonics [1], electronics [2], solar cells [3], memory storage devices [4] and field effect transistors [5]. For these purposes transparent conducting oxide (TCO) nanocrystals (NCs), such as ZnO, SnO_2, In_2O_3 and Ga_2O_3, have emerged as excellent candidates due to their adjustable properties affecting photoluminescence, optical transparency, and electrical conductivity. In particular, the tunable photoluminescence properties of some nanocrystals are attractive for optoelectronic devices such as light emitting diodes (LEDs) [1].

Structural defects are responsible for many properties of nanocrystals [6, 7] making it necessary to understand and control the formation of these defects. However, the role of NC size, surface area, and synthesis conditions in defect formation remains poorly explored. In the past it was assumed that nanocrystals were largely defect free, because their small volume allowed defects to migrate to the surface and be expelled [8]. However, growing evidence suggest that defects play an important role in the properties of nanocrystals [9]. The emergence of nanostructured materials in technology, especially in semiconductor devices, demands a more thorough understanding of the formation and properties of defects in these nanomaterials.

Among TCOs, Ga_2O_3 has one of the largest band gaps ($E_g \approx 4.9$ eV)[10], high electrical conductivity, and strong blue photoluminescence. This combination of properties, arising from the presence of native defects makes Ga_2O_3 interesting for opto-electronic

applications. The photoluminesence, which will be the focus of this thesis, is due to the recombination of an electron trapped on a donor with a hole trapped on an acceptor [7]. Understanding these interactions will allow for tuning of the optical properties of Ga_2O_3 nanocrystals, making them ideal candidates for white-light emitting diodes.

LEDs are particularly interesting because of their potential to revolutionize the lighting industry. Incandescent and fluorescent bulbs have been the main sources of lighting for the past century. Incandescent bulbs are inexpensive but have an efficacy of only 15 lm/W. They convert only about 5% of their input electricity into light, and have an average lifetime of only 1000 hours. Fluorescents bulbs are slightly better, with an efficacy of 65-100 lm/W. However, the mercury used to make them can be harmful to the environment if not disposed of correctly, and their efficacy is unlikely to exceed 100 lm/W [11]. The inefficiency of current lighting technology has lead to a demand for improved light sources, the most promising of which are LEDs. LEDs use 90% less energy than incandescent bulbs and have a lifetime of up to 50,000 hours [12].

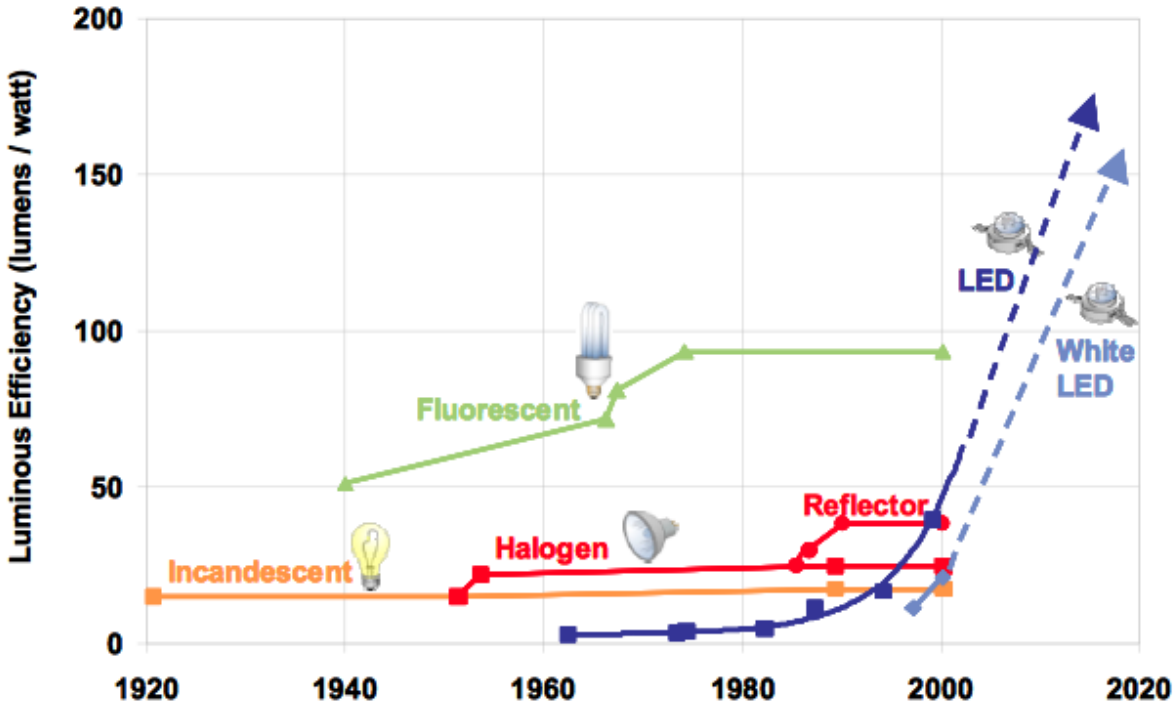

Figure 1.1: Historical and predicted efficacy of different light sources (Image from [11])

Size-dependent decay dynamics of defect-based photoluminescence was studied in colloidal Ga_2O_3 nanocrystals[13, 14]. Theoretical modelling of this decay in the framework of the donor-acceptor pair (DAP) model will be discussed. The original DAP model, which was developed for a large volume of bulk material, has been adapted to include the influence of the geometry of the nanocrystal[15, 16].

Applied mathematics is a key part to studying physical systems such as this one. At it's core applied mathematics seeks to make predictions of physical phenomena, by creating and studying models of physical systems. In order to be useful, these models must balance realism and simplicity. The models must be realistic in order to produce accurate predictions of the system but simple enough to study and manipulate. Finding a solution to a model can be done either analytically or numerically depending on the complexity of the model.

This work was done in collaboration with Paul Stanish, Zoran Miskovic, and Pavle Radovanovic. Experimental data was collected by Paul Stanish. This builds on previous work by Manu Hegde [14] and Ting Wang [17].

1.2 Outline of Thesis

In Section 1.3 we give a brief introduction to the physics of semiconductors, luminescence and the DAP model. In Section 1.4 we describe the nanocrystal synthesis and experimental procedure for measuring photoluminescence at both early and late times. In Chapter 2 we develop a statistical model to describe the photoluminescence decay dynamics. We explore several different cases for the geometry of the nanocrystal and calculate the resulting light emission. We analyze a 3D model where the donors and acceptors are distributed throughout the nanocrystal, and a 2D model where they are restricted to the surface. In Chapter 3 we fit the models to experimental data, using a modified least squares procedure, and discuss trends in the fitting parameters. In Chapter 4 we develop a model for the spectrum of emitted light, using the distribution of donor acceptor separations and the dielectric mismatch between the nanocrystal and its surroundings. In Chapter 5 we use a Monte Carlo algorithm to generalize our model. Donor distributions are generated and the resulting photoluminesence is calculated. Finally in Chapter 6 we summarize our findings and discuss future work. The Matlab code for the Monte Carlo simulation is included in Appendix A.

1.3 Solid State Physics

1.3.1 Semiconductors

The electrical properties of semiconductors differ from those of metals and insulators due to the structure of their energy bands and the location of the Fermi level. In metals, the Fermi level resides inside an energy band so it has many partially filled quantum states which allow for easy conductivity. Conversely, insulators have their Fermi level within a large band gap. The valence band below the Fermi level is full, while the conduction band above the Fermi level is empty. Electrons cannot easily cross this gap so the insulator does not conduct electricity.

In semiconductors the Fermi level resides within a band gap, however the size of the gap is much smaller than in an insulator. Therefore, even at room temperature, the valence band can be thermally populated with electrons. Furthermore, semiconductors may contain impurities which alter their electrical properties. Donor impurities provide an extra electron and create an energy band, or isolated states, below the conduction band. Acceptor impurities provide a vacant state, or electron hole, and create an energy band, or isolated states, above the valence band. These impurities are generally due to foreign atoms which contain a different number of valence electrons than the host.

Semiconductors with large band gaps are interesting for a number of reasons. They absorb and emit light at shorter wavelengths than other semiconductors which allowed blue light emitting diodes to be developed. This in turn led to the development of white light emitting diodes since red, green, and blue LEDs can now be combined. Optical devices made from semiconductors are smaller, more efficient, and have longer lifetimes than those made from other materials.

1.3.2 Photoluminescence

Photoluminescence (PL) is the emission of light from a substance, after the absorbtion of a photon [18]. It is caused by an electron in an excited state falling to a lower vacant energy state accompanied by the emission of a photon. Time scales for this process can vary quite widely, but are usually on the order of a few nanoseconds. The material consists of a host lattice of atoms, sometimes with impurities. There are many mechanisms which cause photoluminescence, but here we will focus on donor-acceptor pair radiative recombination. This is found in semiconductors with impurities that act as donors and acceptors.

The quantity of interest in PL experiments is the intensity of emitted light. We are interested in how the intensity decays over time, $I(t)$, and how the intensity is distributed over wavelengths, $I(\lambda)$, also called the spectrum. Measurements are performed by exciting a sample with a laser pulse. The pulse needs to have a width smaller than the decay time of the of the sample, and the detectors need to be able to resolve ns time scale [19].

1.3.3 Donor Acceptor Pair Radiative Recombination

Here we describe the mechanism which produces the photoluminescence [18].

1. An electron in the valence band becomes excited by incoming radiation and jumps to the conduction band, leaving behind a hole. The system gains energy equal to the band gap energy, $E_g \approx 4.9$ eV [10]. Note that any extra energy from the photon greater than the band gap energy is released in the form of phonons.

2. The electron is captured by an ionized donor, releasing energy in the form of phonons. The energy released is $E_D - e^2/(4\pi\epsilon r)$, where $E_D \approx 0.2$ eV [20] is the donor binding energy relative to the bottom of the conduction band and r is the distance between the donor and acceptor. The Coulomb term originates from the electrostatic interaction between the electron and the negatively charged acceptor.

3. The hole is captured by an ionized acceptor, also releasing energy in the form of phonons. The energy released is equal to the acceptor binding energy, $E_A \approx 0.4$ eV [21], relative to the top of the valence band. This step does not contain a Coulomb term because the donor was neutralized in the previous step.

4.Finally, the electron jumps to the acceptor, recombining with the hole. This step is known as radiative recombination and results in the emission of a photon, not necessarily of the same wavelength as the incoming photon. The energy of the emitted photon is equal to the energy remaining in the system,

$$E_{\text{photon}} = E_g - (E_A + E_D) + e^2/(4\pi\epsilon r). \tag{1.1}$$

This process is outlined in Figure 1.2. Note that this expression is an approximation which is valid for large donor-acceptor separation in bulk material. In Chapter 4 we derive a correction to the Coulomb term for nanocrystals, which have small donor-acceptor separation. The transition rate for this recombination process is given by [22]

$$W(r) = W_{\max} e^{-2r/R_D} \tag{1.2}$$

where r is the distance between donor and acceptor, $W_{\max}$ is the maximum transition rate, and R_D is the donor Bohr radius. This expression is derived by first computing the matrix element between donor and acceptor states, with the assumption that one of them (say, the donor) has a much smaller binding energy than the other [22]. Then the wavefunction of the acceptor can be approximated by a Dirac delta function simplifying the calculation. Note that this assumption is rather poor given the values of E_A and E_D quoted above. The transition rate is then computed from this matrix element using Fermi's golden rule. A more thorough derivation is given in Appendix C.

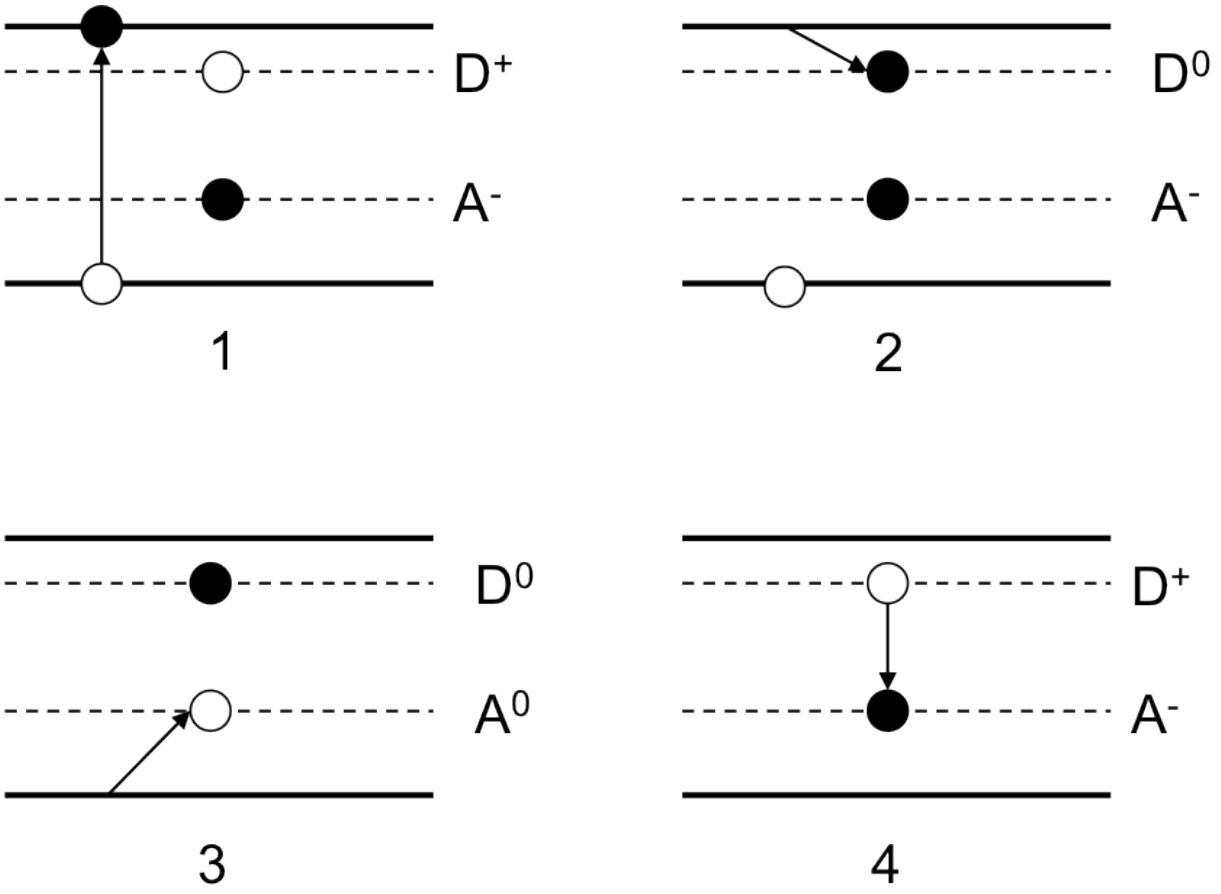

Figure 1.2: Process of donor-acceptor pair radiative recombination. Dotted lines indicate donor (D) and acceptor (A) energy levels with superscripts indicating charge. The top line in each figure is the bottom of the conduction band, and the bottom line is the top of the valence band. (Adapted from [18])

1.4 Experimental Procedure

1.4.1 Nanocrystal Synthesis

The following procedure was used to synthesize Ga_2O_3 nasnocrystals of different sizes [17]. 0.5 g of gallium acetylacetonate ($Ga(acac)_3$) precursor was mixed with 7.0 g of oleylamine in a 100 ml flask. This mixture was raised to 80 °C allowing the acetylacetonate to fully dissolve. The solution was heated at an average rate of 3 °C/min, to a final temperature of between 200 °C and 310 °C, while continuously stirring under a flow of argon.

The final temperature at this step determined the average size of the resulting nanocrystals. Heating to 200 °C produced crystals with a diameter of 3.3 ± 0.5 nm while heating to 310 °C produced crystals with a diameter of 6.0 ± 1.1 nm. The temperature of the synthesis determines the kinetic energy of the system and therefore the rate at which the precursor dissolves. This controls the speed at which nanocrystals grow, which is why higher temperatures result in larger crystals. Another way to increase the size is to allow the reaction to go on longer. This gives the nanocrystals more time to grow.

The mixture was then refluxed for 7 hours at this temperature. The resulting nanocrystals were precipitated with ethanol and placed in a centrifuge for 5 minutes at 3000 rpm. The white powder obtained from this process was washed 3 times with ethanol and placed in the centrifuge a second time. Finally, the nanocrystals were capped with tri-*n*-octylphosphine oxide and dispersed in hexane or toluene. Figure 1.3 shows a transmission electron microscope image of nanocrystals synthesized at 310 °C.

1.4.2 Early Time Experiment - Time Correlated Single Photon Counting

For the early time experiment a high sampling speed is required, necessitating the use of Time Correlated Single Photon Counting (TCSPC). The TCSPC procedure, described in Reference [19], begins by exciting the sample with a pulse of light from an ultrafast laser. The conditions of this excitation are adjusted such that less than one photon is detected per laser pulse. Typically only 1 photon is detected per 100 excitation pulses. This is because the detector is not fast enough to measure multiple photons per pulse when decay time are less than about 1 μs. The time between the excitation pulse and photon detection is stored in a histogram. Since the detection rate is much less than 1 photon per excitation pulse, this histogram represents the waveform of the decay. A higher detection rate would

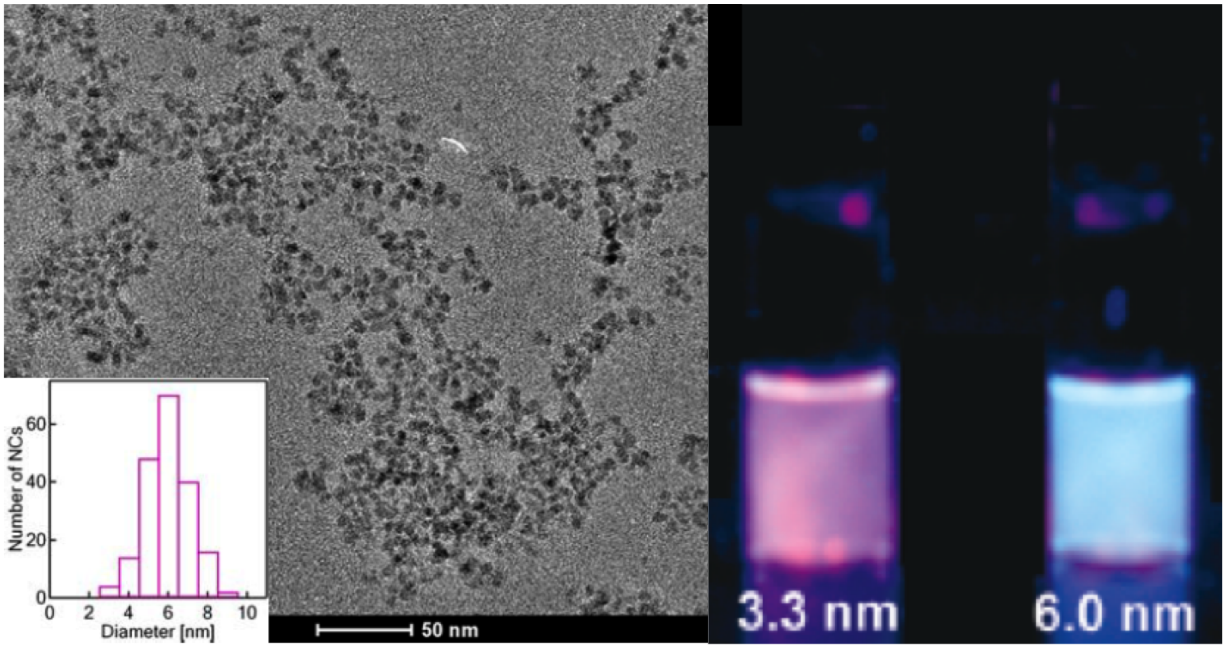

Figure 1.3: Left: Transmission electron microscope image of Ga_2O_3 nanocrystals synthesized at 310 °C. Graph on the bottom left shows nanocrystal size distribution with average diameter of 6.0 ± 1.1 nm. Right: Photograph of 3.3 nm and 6.0 nm Ga_2O_3 nanocrystals illuminated with 250 nm ultraviolet light. (Image from [17])

cause the histogram to be biased towards shorter times because only the first photon per pulse, the one with the shortest time difference, would be detected.

To measure the delay time between excitation and emission the following electronic setup is used. A laser pulse simultaneously excites the sample and sends a signal to the electronics. The signal is passed through a constant function discriminator (CFD) which measures arrival time, and then sends a signal to a time-to-amplitude converter (TAC) which generates a voltage ramp that increases linearly with time on a nanosecond time scale. At some point the sample will emit a photon, sending a signal to another CFD, which then tells the TAC to stop the voltage ramp. The voltage contained in the TAC, which is now proportional to the time delay between excitation and emission, is amplified by a programmable gain amplifier (PGA), and converted to a numerical value by an analog-to-digital converter (ADC). In order to minimize false readings a window discriminator (WD) is used to restrict the the signal to a range of voltages. A histogram of the number of photons emitted for each delay time is created by repeating this procedure many times,

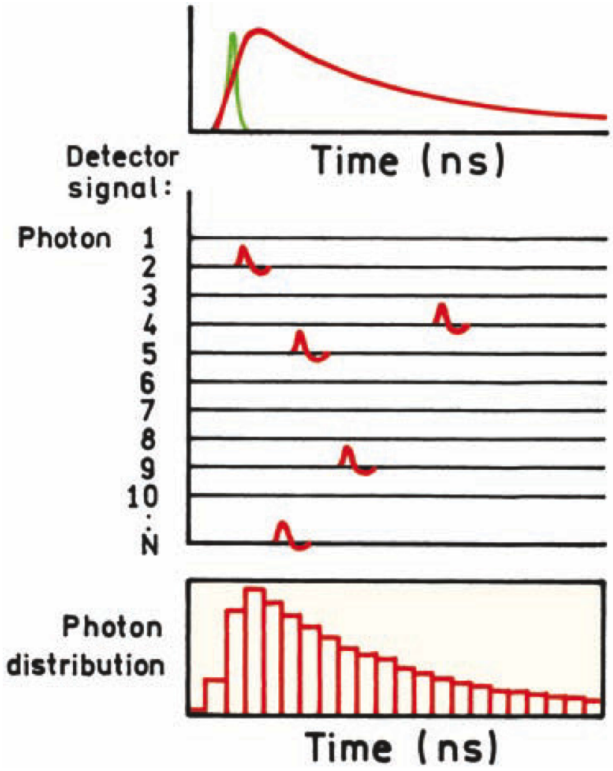

Figure 1.4: Top: Intensity waveforms. Green curve is laser pulse, red curve is signal from sample. Middle: Output of constant function discriminator which measures arrival time of signal. Bottom: Histogram of time delays between excitation and emission, representing waveform of decay. (Image from [19])

see Figure 1.4. This histogram represents the intensity of the emission over time. The electronic set up for this process is shown in Figure 1.5.

1.4.3 Late Time Experiment - Fluorescence Spectrometry

For the late time experiment the nanocrystals were excited using a xenon flash lamp emitting 249 nm ultraviolet light. The data were collected using a Varian Cary Eclipse fluorescence spectrometer with an initial delay of 4 μs to avoid contamination of the signal from the lamp. Each data point is collected over an acquisition time of $\Delta t = 1\mu$s.

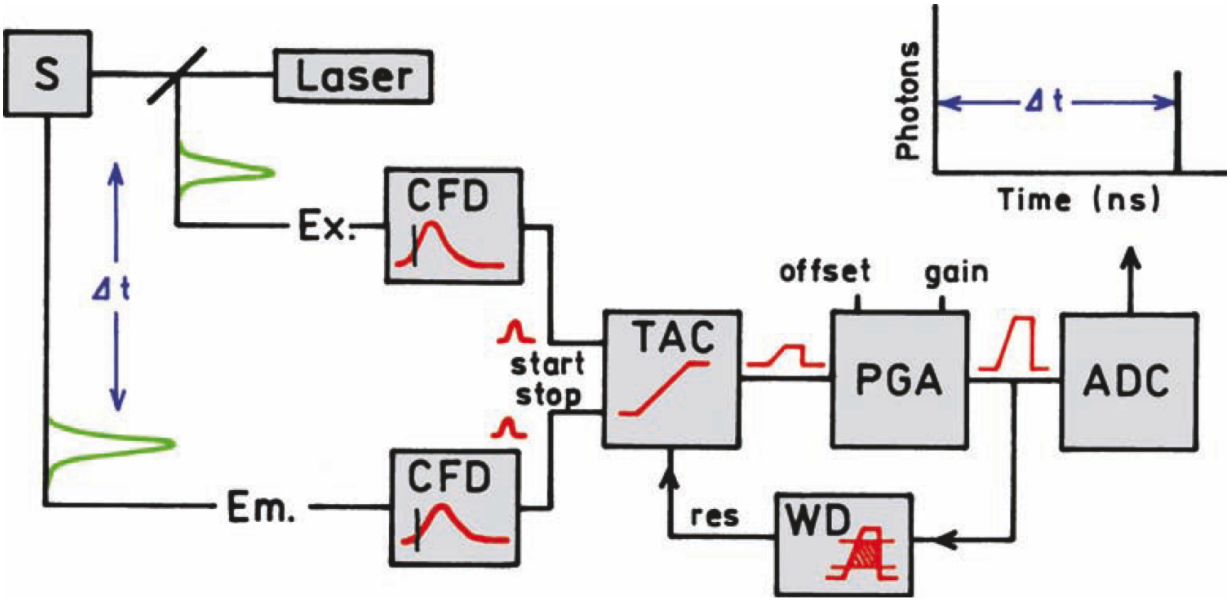

Figure 1.5: Schematic diagram of electronics for Time Correlated Single Photon Counting (TCSPC). Laser excites sample (S) and sends signal to constant function discriminator (CFD) which causes the time-to-amplitude converter (TAC) to begin generating a voltage ramp. Photon emitted from sample is sent to another CFD which tells the TAC to stop the voltage ramp. Voltage in TAC is sent to a programmable gain amplifier (PGA) and converted to a numerical value by an analog-to-digital converter (ADC). Window discriminator (WD) is used to minimize false readings. (Image from [19])

Chapter 2

Analytical Model for Decay Dynamics

2.1 Nanocrystal Population Decay Dynamics

Suppose we have a population of nanocrystals which have all been excited by a laser pulse, and that the number of excited nanocrystals, N, decays at a rate proportional to the number of remaining excited crystals. Then N obeys the differential equation

$$\frac{dN}{dt} = -\gamma N, \tag{2.1}$$

where γ is the decay rate, and the initial condition is $N(0) = N_0$, the initial excited population. This results in an exponential decay of the excited crystal population,

$$N(t) = N_0 e^{-\gamma t}. \tag{2.2}$$

In experiments the observed quantity is not the number of excited crystals, but rather the intensity of emitted light. These are however directly proportional, so we can simply substitute $N(t)$ and N_0 with $I(t)$ and I_0 cancelling any proportionality constant.

$$I(t) = I_0 e^{-\gamma t} \tag{2.3}$$

The lifetime is the average amount of time that a nanocrystal remains in the excited state after becoming excited. The lifetime can be calculated by averaging t over the number of

excited nanocrystals.

$$\begin{aligned}\langle t \rangle &= \frac{\int_0^\infty tN(t)dt}{\int_0^\infty N(t)dt} \\ &= \frac{1}{\gamma}\end{aligned} \tag{2.4}$$

So the average lifetime is the inverse of the decay rate. This macroscopic model does not tell us anything about the nanocrystals themselves. For that purpose we need to develop a microscopic model which depends on the properties of the crystals.

2.2 Statistical Model for Individual Nanocrystal Decay Dynamics

We assume that the processes taking place in different nanocrystals are independent of each other. In that way, the large population of crystals in the sample provides an ensemble that allows us to study the properties of nanocrystals at the statistical level. To gain more information about the microscopic properties of the nanocrystals we need to develop a model which depends on these properties. We assume that each nanocrystal contains a single acceptor and an excess of donors. Let n be a random number representing the number of donors in a nanocrystal, and let $\{\vec{r}_j\}_{j=1}^n$ be a set of random radius vectors representing the positions of those donors [22]. See Figure 2.1 for a diagram of donors and acceptor.

Let $Q(t)$ be the probability that the acceptor is available for electron capture. The rate of change of $Q(t)$ is equal to the probability that the acceptor is available multiplied by the sum of the transition rates for all donors. This leads to the differential equation

$$\frac{dQ(t)}{dt} = -Q(t)\sum_{j=1}^{n} W(r_j), \tag{2.5}$$

where $W(r)$ is the donor-acceptor recombination rate, which depends on the donor-acceptor distance r. The initial condition is $Q(0) = 1$ since the electron is initially in the excited state, meaning the acceptor is available for electron capture. The solution to this equation

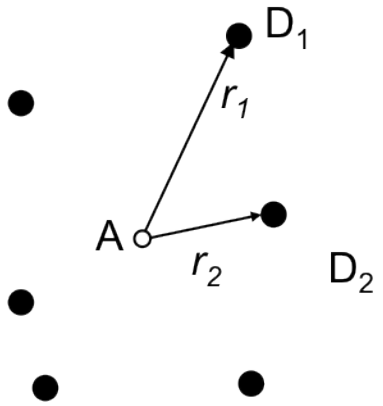

Figure 2.1: A single acceptor and a random number of donors $\{D_1,\ D_2,\ \ldots, D_n\}$ with random positions $\{\vec{r}_1, \vec{r}_2, \ldots, \vec{r}_n\}$.

is,

$$\begin{aligned} Q(t) &= \exp[-t\sum_{j=1}^{n} W(r_j)] \\ &= \prod_{j=1}^{n} \exp[-tW(r_j)]. \end{aligned} \tag{2.6}$$

2.2.1 Position of Donors

The joint probability distribution function (PDF) $f_n(\vec{r}_1, \vec{r}_2, ..., \vec{r}_n)$ gives the probability that donor j occupies a small volume $d^3\vec{r}_j$ (or surface area $d^2\vec{r}_j$) about the position $\vec{r}_j$. We will assume that the donors do not interact with each other, so the n^{th} order PDF can be written as the product of first order PDF's.

$$f_n(\vec{r}_1, \vec{r}_2, ..., \vec{r}_n) = f_1(\vec{r}_1) f_1(\vec{r}_2) ... f_1(\vec{r}_n) \tag{2.7}$$

Each first order PDF is normalized so that $\int f_1(\vec{r}_j) d^N\vec{r}_j = 1$. Where the integral is taken over the entire volume ($N = 3$) or the surface area ($N = 2$) of the nanocrystal, depending

on the model chosen. Taking the average of $Q(t)$ over the positions $\vec{r}_j$ we obtain

$$\begin{aligned}\langle Q(t)\rangle &= \int \cdots \int Q(t)[f_1(\vec{r}_1)\ldots f_1(\vec{r}_n)]d^N\vec{r}_1\ldots d^N\vec{r}_n \\ &= \left[\int f_1(\vec{r})e^{-tW(r)}d^N\vec{r}\right]^n \end{aligned} \tag{2.8}$$

where angled brackets denotes spatial average.

2.2.2 Number of Donors

We will assume that the number of donors is Poisson distributed with average μ. This is motivated by the fact that replacing lattice sites with defects follows a binomial distribution which tends towards the Poisson distribution when the probability of replacement is small [16, 15]. The probability distribution for the number of donors is therefore,

$$p_n = e^{-\mu}\frac{\mu^n}{n!}. \tag{2.9}$$

Taking the average of $\langle Q(t)\rangle$ over the number of donors, n, we obtain

$$\begin{aligned}\overline{\langle Q(t)\rangle} &= \sum_{n=0}^{\infty} p_n\langle Q(t)\rangle \\ &= \exp\left[\mu\int f_1(\vec{r})(e^{-tW(r)}-1)d^N\vec{r}\right] \end{aligned} \tag{2.10}$$

where the overbar denotes average over number of donors.

2.2.3 Exclusion Distance

The model specified so far assumes that the donors and acceptor are point particles. However, real molecules have non-zero size and therefore cannot be located arbitrarily close to one another. We will include an exclusion distance, R_{ex}, about the acceptor where donors cannot be located. This has the effect of eliminating the fastest recombinations from the possible configurations and therefore slows down the decay at early times.

To proceed further we need to specify $f_1(\vec{r})$, the first order PDF for the spatial distribution of donors. Donor-acceptor exclusion can be easily included in the model by specifying

that $f_1(\vec{r}) = 0$ when $r < R_{ex}$. Donor-donor exclusion however cannot be added in this way. This is because the separation of the n_{th} order PDF into a product of first order PDF's required that the donors be independent. Donor-donor exclusion breaks this assumption and would therefore require a full n_{th} order PDF. Numerical methods could be used for this situation, but for now we proceed analytically with only donor-acceptor exclusion.

2.2.4 Intensity of Emitted Light

In order to compare this model with experiment we must obtain the intensity of the emitted light, $I(t)$. In this context, intensity is a measure of the number of photons emitted per unit time. This is given by the total transition rate, $\sum_{j=1}^{n} W(r_j)$, multiplied by the probability that the acceptor is available for recombination to occur, $Q(t)$. From Equation 2.5 we can see that this gives the expression

$$I(t) = -\frac{d\overline{\langle Q(t)\rangle}}{dt}. \tag{2.11}$$

However, for the late time experiments the acquisition time is large ($\Delta t = 1\mu$s), so this must be modified to

$$I^{late}(t) = \frac{\overline{\langle Q(t)\rangle} - \overline{\langle Q(t+\Delta t)\rangle}}{\Delta t}. \tag{2.12}$$

It is informative to look at the sign of the intensity and it's derivatives. differentiating Equation 2.10 gives

$$I(t) = \mu \int f_1(\vec{r}) W(r) e^{-tW(r)} \overline{\langle Q(t)\rangle} d^N\vec{r} \geq 0. \tag{2.13}$$

Since $f_1(\vec{r})$, $W(r)$, $e^{-tW(r)}$, and $\overline{\langle Q(t)\rangle}$ are all non-negative, the intensity is always non-negative. Differentiating 2.13 gives

$$\frac{dI(t)}{dt} = -\mu \int f_1(\vec{r}) W(r) e^{-tW(r)} [W(r)\overline{\langle Q(t)\rangle} + I(t)] d^N\vec{r} \leq 0. \tag{2.14}$$

This is the integral of non-negative functions multiplied by a negative quantity, so the intensity is always decreasing. Differentiating once more gives

$$\frac{d^2I(t)}{dt^2} = \mu \int f_1(\vec{r}) W r e^{-tW(r)} [W(r)^2\overline{\langle Q(t)\rangle} + 2W(r)I(t) - \frac{dI(t)}{dt}] d^N\vec{r} \geq 0, \tag{2.15}$$

which is also non-negative. So this model gives a function for intensity which is positive, decreasing, and concave up. These features, while not strictly necessary, are consistent with the experimental data considered here.

2.3 Model 1: Macroscopic Limit

The first model presented here is the so called Thomas model first derived in Reference [22]. It does not include a random number of donors or an exclusion distance. Instead, we go to the macroscopic limit by allowing the number of donors, and the volume of the nanocrystal to approach infinity while keeping the number density of donors constant. We place the acceptor in the center of a nanocrystal with radius R_c and the donors uniformly distributed throughout the volume. The PDF for this is

$$f_1(\vec{r}) = \left\{ \begin{array}{ccc} 1/V & : & 0 < r < R_c \\ 0 & : & \text{Otherwise} \end{array} \right\}, \tag{2.16}$$

where $V = \frac{4}{3}\pi R_c^3$ is the volume of the nanocrystal. We insert this into Equation 2.8 and replace $1/V$ with n_D/n where n_D is the number density of donors in the nanocrystal. This gives

$$\overline{\langle Q(t) \rangle} = \left[1 + \frac{n_D}{n} \int (e^{-tW(r)} - 1) d^3\vec{r} \right]^n \tag{2.17}$$

Now, we let n and V go to infinity while keeping $n_D = n/V$ constant. Using the fact that $(1 + x/n)^n \to e^x$ as $n \to \infty$ we get

$$\overline{\langle Q(t) \rangle} = \exp \left[n_D \int (e^{-tW(r)} - 1) d^3\vec{r} \right] \tag{2.18}$$

The assumption of large volume and number of defects is somewhat unsatisfactory, so in the following models we will include a random number of donors and a fixed volume.

2.4 Model 2: Maximum Exclusion

Here we consider a simple model where the acceptor is at the center of the nanocrystal and the donors are restricted to the surface. This is equivalent to saying that the exclusion distance is equal to the radius of the nanocrystal. This model has the property that the transition rate is a constant given by $W = W(R_c) = W_{max} e^{-2R_c/R_D}$. Inserting this into Equation 2.6 we get

$$Q(t) = e^{-nWt}. \tag{2.19}$$

Since this has no spatial dependence we only need to average over number of donors, which gives

$$\overline{Q(t)} = \exp[\mu(e^{-Wt} - 1)]. \tag{2.20}$$

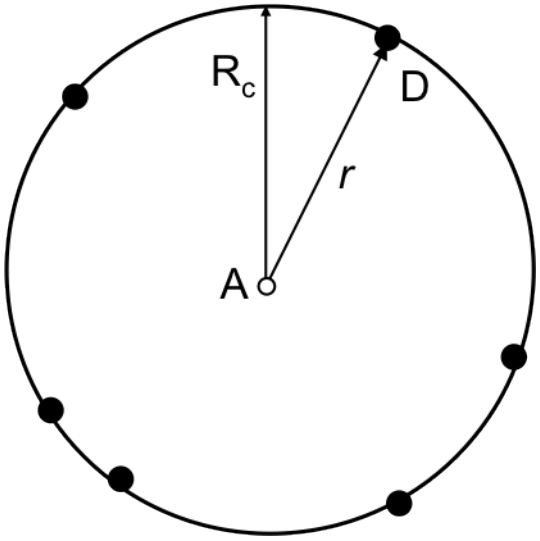

Figure 2.2: Maximum exclusion model with acceptor at the center of the nanocrystal and donors uniformly distributed on the surface.

Differentiating to get the intensity gives

$$I(t) = \mu W e^{-Wt} \exp[\mu(e^{-Wt} - 1)]. \tag{2.21}$$

2.5 Model 3: 3D

Next we consider a 3D model with the acceptor in the center of the nanocrystal and the donors uniformly distributed throughout the volume. The nanocrystal has radius R_c and an exclusion radius, R_{ex}, about the acceptor where the donors cannot be located. Using the fact that the PDF must be normalized, we get that

$$f_1(\vec{r}) = \left\{ \begin{array}{ccc} [\frac{4}{3}\pi R_c^3(1 - \frac{R_{ex}^3}{R_c^3})]^{-1} & : & R_{ex} \leq r \leq R_c \\ 0 & : & \text{Otherwise} \end{array} \right\}.$$

Inserting this into equation 2.10 and using $W(r) = W_{\max} e^{-2r/R_D}$ we get

$$\overline{\langle Q(t) \rangle} = \exp\left\{ \frac{3\mu}{R_c^3 - R_{ex}^3} \int_{R_{ex}}^{R_c} [\exp(-tW_{\max} e^{-2r/R_D}) - 1] r^2 dr \right\}. \tag{2.22}$$

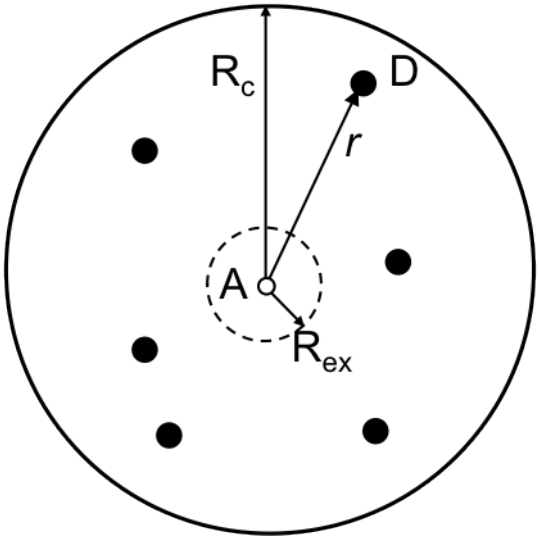

Figure 2.3: 3D model with acceptor in the center of the nanocrystal and donors uniformly distributed throughout the volume. Donors cannot be located within the dotted circle of radius R_{ex}.

Now let $x = r/R_c$, $\tau = tW_{\max}$, $\rho = R_c/R_D$, and $\epsilon = R_{ex}/R_c$. Then, integrating by parts we get

$$\overline{\langle Q(t)\rangle} = \exp\left\{\frac{3\mu}{1-\epsilon^3}\left[e^{-\tau e^{-2\rho}} - 1 - \epsilon^3(e^{-\tau e^{-2\rho\epsilon}} - 1) - 2\rho\tau J_3^{(3D)}\right]\right\} \tag{2.23}$$

where

$$J_i^{(3D)} = \int_\epsilon^1 x^i e^{-2\rho x} e^{-\tau e^{-2\rho x}} dx. \tag{2.24}$$

To get an expression for the intensity of the emitted light we differentiate Equation 2.23 with respect to t.

$$I(t) = \frac{3\mu W_{\max}}{1-\epsilon^3} J_2^{(3D)} \exp\left\{\frac{3\mu}{1-\epsilon^3}\left[e^{-\tau e^{-2\rho}} - 1 - \epsilon^3(e^{-\tau e^{-2\rho\epsilon}} - 1) - 2\rho\tau J_3^{(3D)}\right]\right\} \tag{2.25}$$

If the exclusion radius, R_{ex}, is much smaller than the radius of the nanocrystal, R_c, then $\epsilon \to 0$ and this simplifies to

$$I(t) = 3\mu W_{\max} J_2^{(3D)} \exp[3\mu(e^{-\tau e^{-2\rho}} - 1 - 2\rho\tau J_3^{(3D)})] + \mathcal{O}(\epsilon^3), \tag{2.26}$$

which is the expression in Reference [14].

2.6 Model 4: 2D

Next we will consider a 2D model where the acceptor and donors are distributed on the surface of the nanocrystal. The spatial PDF for this model is given by

$$f_1(\vec{r}) = \left\{ \begin{array}{ccc} [4\pi R_c^2(1-\frac{R_{ex}^2}{4R_c^2})]^{-1} & : & 0 \leq \theta \leq \theta_{\max} \\ 0 & : & \text{Otherwise} \end{array} \right\}$$

where $\theta_{\max} = \arccos(\frac{R_{ex}}{2R_c})$.

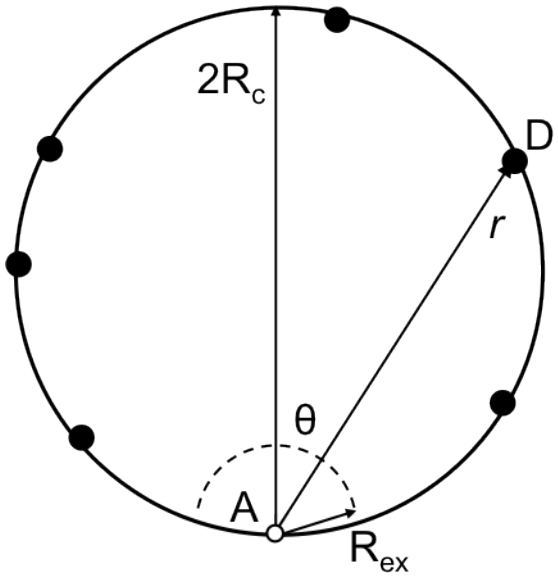

Figure 2.4: 2D model with acceptor on the surface of the nanocrystal and donors uniformly distributed on the surface. Donors cannot be located within the dotted circle of radius R_{ex}.

In this model the separation between the donor and acceptor is determined by the angle formed between the line connecting the two, and the main axis of the nanocrystal. Using simple trigonometry we obtain the expression

$$r = 2R_c \cos(\theta). \tag{2.27}$$

Furthermore, the surface element dS is given by

$$dS = 2R_c^2 \sin(2\theta) d\theta d\phi. \tag{2.28}$$

Inserting this and the PDF into Equation 2.10 we get

$$\overline{\langle Q(t)\rangle} = \exp\left\{\frac{\mu}{1 - R_{ex}^2/4R_c^2}\int_0^{\theta_{\max}} [\exp(-tW_{\max}e^{-4R_c\cos(\theta)/R_D}) - 1]2\sin(\theta)\cos(\theta)d\theta\right\}. \tag{2.29}$$

Now let $x = \cos(\theta)$, $\tau = tW_{\max}$, $\rho = R_c/R_D$, and $\epsilon = R_{ex}/2R_c$. Then, integrating by parts we get

$$\overline{\langle Q(t)\rangle} = \exp\left\{\frac{\mu}{1-\epsilon^2}\left[e^{-\tau e^{-4\rho}} - 1 - \epsilon^2(e^{-\tau e^{-4\rho\epsilon}} - 1) - 4\rho\tau J_2^{(2D)}\right]\right\} \tag{2.30}$$

where

$$J_i^{(2D)} = \int_\epsilon^1 x^i e^{-4\rho x} e^{-\tau e^{-4\rho x}} dx. \tag{2.31}$$

To get an expression for the intensity of the emitted light we differentiate Equation 2.30 with respect to t.

$$I(t) = \frac{2\mu W_{\max}}{1-\epsilon^2} J_1^{(2D)} \exp\left\{\frac{\mu}{1-\epsilon^2}\left[e^{-\tau e^{-4\rho}} - 1 - \epsilon^2(e^{-\tau e^{-4\rho\epsilon}} - 1) - 4\rho\tau J_2^{(2D)}\right]\right\} \tag{2.32}$$

If the exclusion radius, R_{ex}, is much smaller than the radius of the nanocrystal, R_c, then $\epsilon \to 0$ and this simplifies to

$$I(t) = 2\mu W_{\max} J_1^{(2D)} \exp\left[\mu\left(e^{-\tau e^{-4\rho}} - 1 - 4\rho\tau J_2^{(2D)}\right)\right] + \mathcal{O}(\epsilon^2), \tag{2.33}$$

which is the expression in Reference [14].

Chapter 3

Fitting Models to Data

3.1 Fitting Parameters

Two separate experiments were required to obtain data for a larger time interval. The first experiment produced data from 0.5μs to about 10μs, while the second produced data from 4μs to about 50μs. In both cases we excluded a portion of the data below an intensity threshold (0.05 and 0.001 respectively) relative to the initial intensity, because the data contained significant noise.

For the 3D case we can make the substitution $y = e^{-2\rho x}$ to get

$$\begin{aligned} J_i^{(3D)} &= \left(\frac{-1}{2\rho}\right)^{i+1} \int_{e^{-2\rho\epsilon}}^{e^{-2\rho}} (\ln y)^i e^{-\tau y} \mathrm{d}y \\ &= \left(\frac{-1}{2\rho}\right)^{i+1} \left(\int_{e^{-2\rho\epsilon}}^{\infty} (\ln y)^i e^{-\tau y} \mathrm{d}y - \int_{e^{-2\rho}}^{\infty} (\ln y)^i e^{-\tau y} \mathrm{d}y \right) \end{aligned} \tag{3.1}$$

Similarly for the 2D case we make the substitution $y = e^{-4\rho x}$ to get

$$J_i^{(2D)} = \left(\frac{-1}{4\rho}\right)^{i+1} \left(\int_{e^{-4\rho\epsilon}}^{\infty} (\ln y)^i e^{-\tau y} \mathrm{d}y - \int_{e^{-4\rho}}^{\infty} (\ln y)^i e^{-\tau y} \mathrm{d}y \right) \tag{3.2}$$

The integrals in Equations 3.1 and 3.2 have closed form solutions in terms of hypergeometric functions so they can be easily evaluated in Maple without integrating numerically.

In the fitting procedure we chose $W_{\max} = 10^7 s^{-1}$ as the most reasonable value [21] and treated μ, R_D, and R_{ex} as free parameters. Using the least squares method, we computed the error as

$$Error = \sum_i (I(t_i) - I_i)^2, \tag{3.3}$$

where (t_i, I_i) is the i^{th} data point. This was done separately for the early and late data, and they were combined with the late data given 10 times the weight of the early data. The reason for this was that the early data had a higher variance. The error was then minimized as a function of $\mu, R_D,$ and R_{ex}. The results are shown in Table 3.1 for 3 different sizes of nanocrystals and for both 2D, 3D and maximum exclusion models.

Table 3.1: Fitting parameters obtained for the best overall fit of 3D, 2D, and maximum exclusion models to the experimental data.

	3D Model			2D Model			Maximum Exclusion	
R_c(nm)	μ	R_D(nm)	R_{ex}(nm)	μ	R_D(nm)	R_{ex}(nm)	μ	R_D(nm)
1.55	6.6	0.91	1.5	10	1.5	2.7	2.7	2.6
2.1	6.8	0.73	0.92	10	1.2	1.7	2.7	2.7
2.75	3.3	1.0	1.4	4.1	1.9	3.0	2.4	2.8

3.2 Plots

Here we plot the intensity decay curves using the best fit parameters along with the experimental data. The maximum exclusion model produces very poor fits at late times, but both 2D and 3D models produce very good fits for both early and late times.

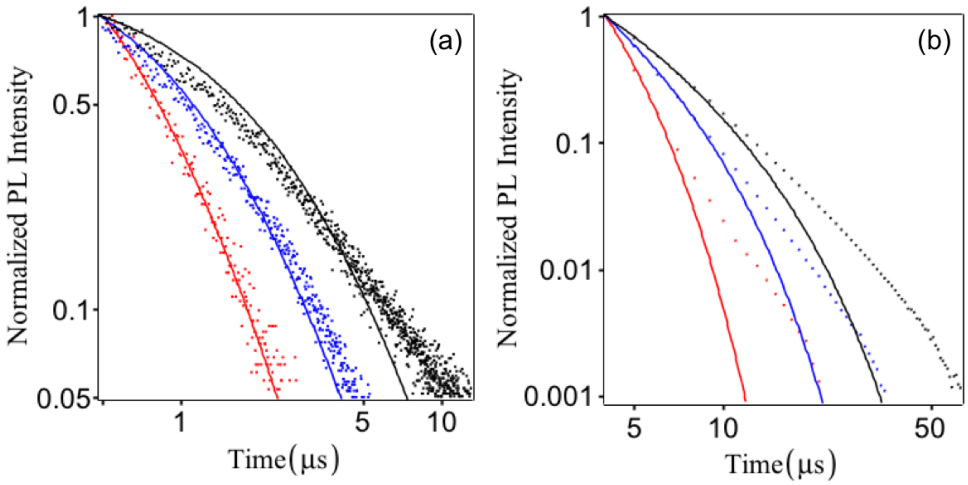

Figure 3.1: Normalized PL intensity and corresponding maximum exclusion model best fit (solid lines) for R_c=1.55 nm (red), 2.1 nm (blue), and 2.75 nm (black). (a) shows early times, (b) shows late times. Both are normalized to one at the initial time of measurement.

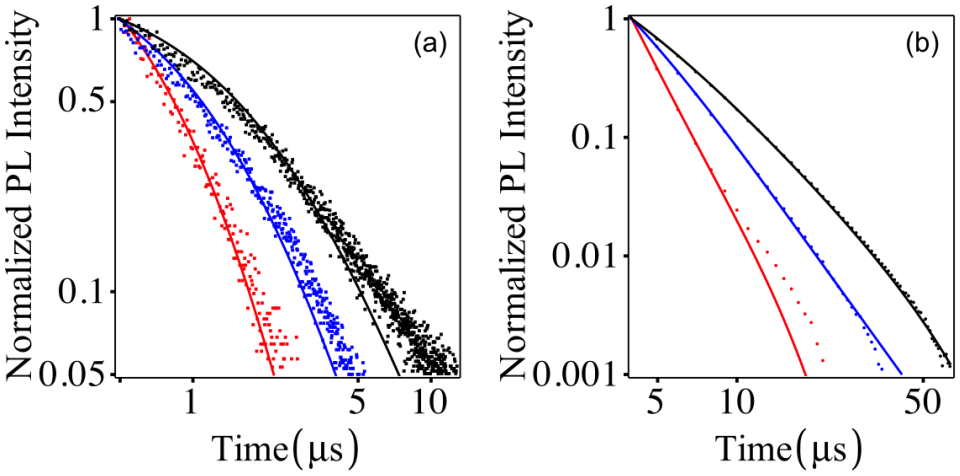

Figure 3.2: Normalized PL intensity and corresponding 3D model best fit (solid lines) for R_c=1.55 nm (red), 2.1 nm (blue), and 2.75 nm (black). (a) shows early times, (b) shows late times. Both are normalized to one at the initial time of measurement.

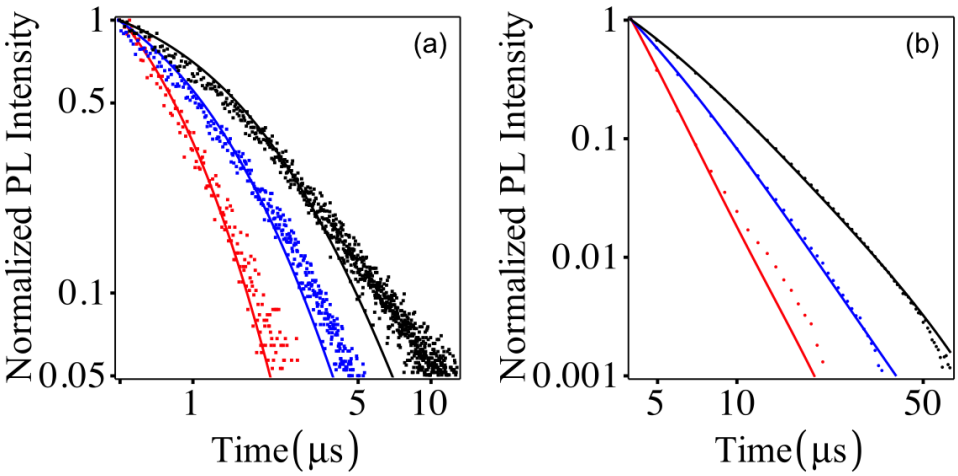

Figure 3.3: Normalized PL intensity and corresponding 2D DAP model best fit (solid lines) for R_c=1.55 nm (red), 2.1 nm (blue), and 2.75 nm (black). (a) shows early times, (b) shows late times. Both are normalized to one at the initial time of measurement.

3.3 Effects of Exclusion Radius

To demonstrate the effect of the exclusion radius we compare curves with different values of R_{ex} in Figure 3.4. Here we show only the 3D case, but the 2D case is similar. At early times the dashed lines, which have no exclusion radius, are steeper. A model with no exclusion radius allows for donors and acceptors to be arbitrarily close together. Those pairs which are very close together have a higher recombination rate, leading to a faster decay while those close pairs are recombining. Those nanocrystals containing close pairs are also the ones which have, on average, a larger number of defects. After these nanocrystals are removed from the sample (because they have undergone recombination), those that are left have, on average, fewer number of defects than those of the model with exclusion. Fewer defects means a greater average distance between defects, which means a slower decay. This is indeed the case in Figure 3.4. The dashed, no exclusion curves become less steep at later times.

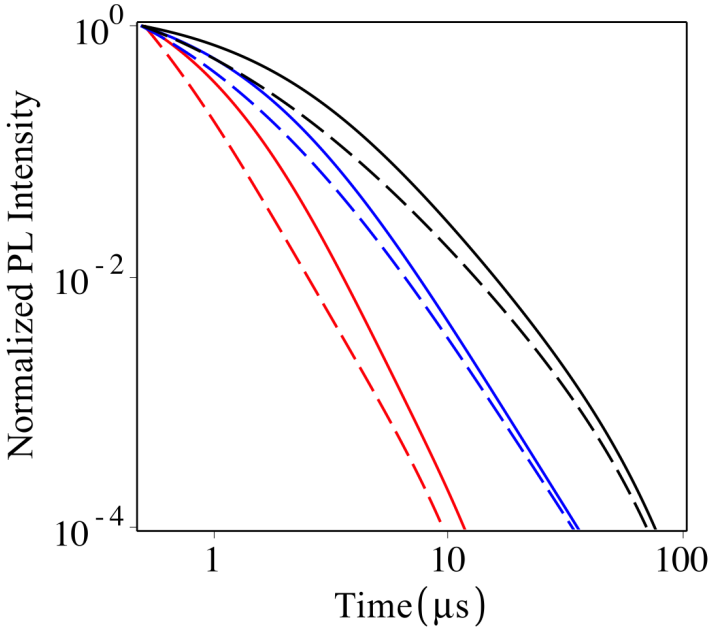

Figure 3.4: Comparison of 3D model decay curves with different values of R_{ex} for R_c=1.55 nm (red), 2.2 nm (blue), and 2.75 nm (black). Solid lines have R_{ex} equal to the best fit values given in Table 3.1. Dashed lines have $R_{ex} = 0$.

Chapter 4

Modelling Spectrum

To model the spectrum we need to develop an expression for the intensity of the light emitted at each wavelength, or equivalently, at each energy. Figure 4.1 shows the observed spectra for three different sizes of nanocrystals. Note that these are time integrated spectra, meaning they represent the total intensity of light emitted at each wavelength over the course of the entire observation time.

4.1 Bare Coulomb Interaction

If we consider only the Coulomb interaction between donor and acceptor, the energy of the emitted photon, E, is related to the distance between donor and acceptor, r, according to the equation

$$E = E_0 + \frac{ke^2}{\epsilon_1 r}, \tag{4.1}$$

where $k = 1/(4\pi\epsilon_0)$, $\epsilon_1 = 10.4$ is the relative permittivity of Ga_2O_3 [23, 5], and $E_0 = E_g - (E_A + E_D) \approx 4.3$ is the effective band gap. Note that E_A is measured from the top of the valence band and E_D is measured from the bottom of the conduction band.

Earlier we stated that the intensity, which is the number of photons emitted per unit time, is given by the total transition rate, $\sum_{j=1}^{n} W(r_j)$, multiplied by the probability that the acceptor is available for recombination to occur, $Q(t)$. To get the intensity at a particular energy we multiply this by the probability that the emitted photon has a particular energy. Since the possible distances between donor and acceptor, and therefore the

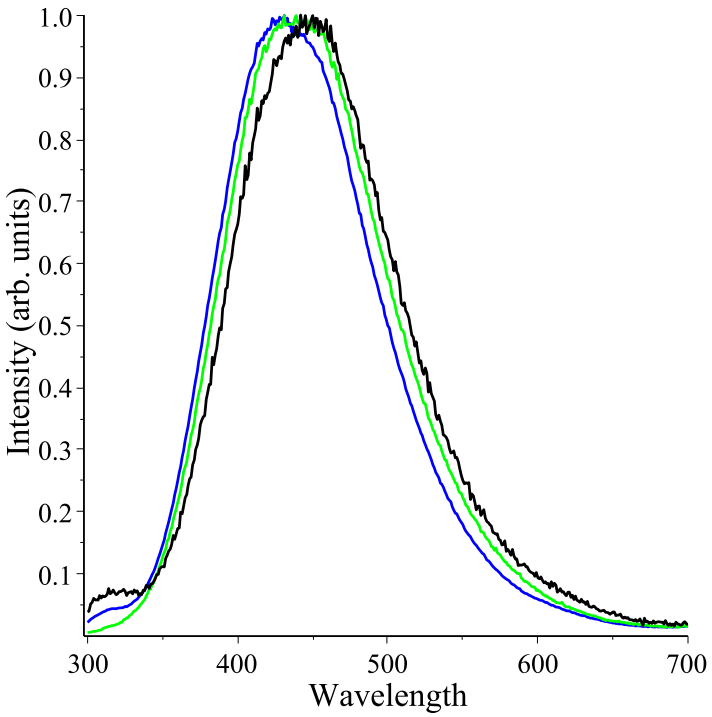

Figure 4.1: Time integrated photoluminescence spectra for two different sizes of Ga_2O_3 nanocrystals. Blue curve has $R_c = 2.1$ nm, green curve has $R_c = 2.45$ nm, black curve has $R_c = 2.75$ nm.

possible energies, form a continuum, this probability is given by a Dirac delta function, $\delta(E - (E_0 + ke^2/\epsilon_1 r_j))$. So the intensity, $D_n(E,t)$, is

$$D_n(E,t) = Q(t) \sum_{j=1}^{n} W(r_j) \delta \left(E - \left(E_0 + \frac{ke^2}{\epsilon_1 r_j} \right) \right), \tag{4.2}$$

where $Q(t)$ is given in Equation 2.6.

As before, we average over the spatial distribution of donors by multiplying by the

spatial PDF and integrating over the volume (or surface area) of the nanocrystal.

$$\begin{aligned}\langle D_n(E,t)\rangle &= \int\cdots\int D_n(E,t)[f_1(\vec{r_1})\dots f_1(\vec{r_n})]d^N\vec{r_1}\dots d^N\vec{r_n} \\ &= \left[\int e^{-W(r)t}f_1(\vec{r})d^N\vec{r}\right]^{n-1} \\ &\quad\times n\int W(r)\delta\left(E-\left(E_0+\frac{ke^2}{\epsilon_1 r}\right)\right)e^{-W(r)t}f_1(\vec{r})d^N\vec{r}. \end{aligned} \tag{4.3}$$

Next we average over the number of donors using a Poisson distribution.

$$\begin{aligned}\overline{\langle D(E,t)\rangle} &= \sum_{n=0}^{\infty} e^{\mu}\frac{\mu^n}{n!}\langle D_n(E,t)\rangle \\ &= \exp\left[\mu\int f_1(\vec{r})(e^{-W(r)t}-1)d^N\vec{r}\right] \\ &\quad\times\mu\int f_1(\vec{r})W(r)e^{-W(r)t}\delta\left(E-\left(E_0+\frac{ke^2}{\epsilon_1 r}\right)\right)d^N\vec{r} \\ &= \overline{\langle Q(t)\rangle}\mu\int f_1(\vec{r})W(r)e^{-W(r)t}\delta\left(E-\left(E_0+\frac{ke^2}{\epsilon_1 r}\right)\right)d^N\vec{r}. \end{aligned} \tag{4.4}$$

As a consistency check we can integrate this expression over all energies and we should arrive at Equation 2.13 which is the intensity over all energies. An integral over all energies only affects the delta function which integrates to 1. What remains is

$$\int_0^{\infty}\overline{\langle D(E,t)\rangle}dE = \exp\left[\mu\int f_1(\vec{r})(e^{-W(r)t}-1)d^N\vec{r}\right]\mu\int f_1(\vec{r})W(r)e^{-W(r)t}d^N\vec{r}, \tag{4.5}$$

which is exactly Equation 2.13 for the integrated intensity. Now we can apply the geometric models in Chapter 2 to the spectrum.

4.1.1 3D Model

The PDF for the 3D model is

$$f_1(\vec{r}) = \left\{\begin{array}{ccc} [\frac{4}{3}\pi R_c^3(1-\frac{R_{ex}^3}{R_c^3})]^{-1} & : & R_{ex}\le r\le R_c \\ 0 & : & \text{Otherwise}\end{array}\right\}.$$

Applying this to Equation 4.4 and using the fact that $\delta(E - E_0 - ke^2/\epsilon_1 r) = \frac{r}{E-E_0}\delta(r - ke^2/\epsilon_1(E - E_0))$ we get

$$\overline{\langle D(E,t)\rangle} = \overline{\langle Q(t)\rangle}\frac{3\mu W_{\max}}{(R_c^3 - R_{ex}^3)(E - E_0)} \times \int_{R_{ex}}^{R_c} \exp\left(\frac{-2r}{R_D} - W_{\max}te^{-2r/R_D}\right)\delta\left(r - \frac{ke^2}{\epsilon_1(E - E_0)}\right)r^3 dr. \tag{4.6}$$

Using the sifting property of the Dirac delta function we evaluate the integral by replacing r with $ke^2/\epsilon_1(E - E_0)$ when $R_{ex} \leq ke^2/\epsilon_1(E - E_0) \leq R_c$. We also perform the change of variables $x = \frac{ke^2}{\epsilon_1 R_c(E-E_0)}$, $\tau = W_{\max}t$, $\rho = R_c/R_D$, and $\epsilon = R_{ex}/R_c$.

$$\overline{\langle D(x,\tau)\rangle} = \overline{\langle Q(t)\rangle}\frac{3\mu W_{\max}R_c\epsilon_1}{ke^2(1 - \epsilon^3)}x^4 \exp\left(-2\rho x - \tau e^{-2\rho x}\right) H(x - \epsilon)H(1 - x) \tag{4.7}$$

where H is the Heaviside step function indicating that the function is 0 outside the interval $[\epsilon, 1]$

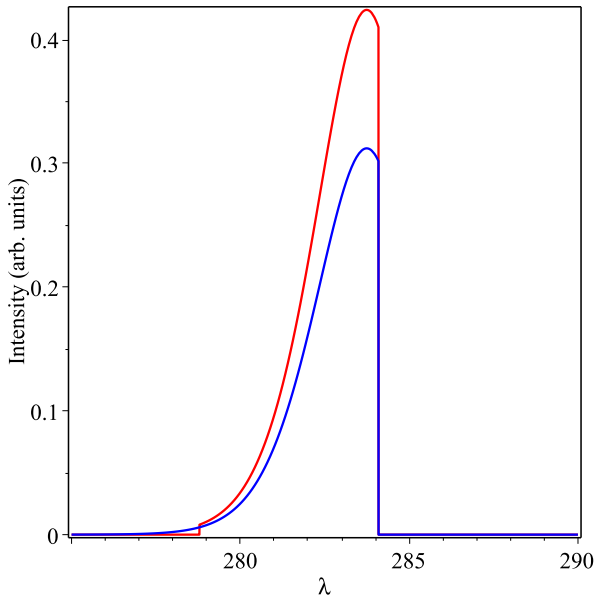

Figure 4.2: Spectrum for $R_c = 2.1$ nm crystals. 3D model at $t = 5$ μs with $E_0 = 4.3$ eV, $\epsilon_1 = 10.4$ and other parameters from Table 3.1. Blue curve has $R_{ex} = 0$.

4.1.2 2D Model

For the 2D model the PDF is

$$f_1(\vec{r}) = \left\{ \begin{array}{ccc} [4\pi R_c^2(1-\frac{R_{ex}^2}{4R_c^2})]^{-1} & : & 0 \leq \theta \leq \theta_{\max} \\ 0 & : & \text{Otherwise} \end{array} \right\}.$$

Applying this to Equation 4.4, using the scaling property of the Dirac delta function, and performing the change of variables $r = 2R_c\cos(\theta)$ we get

$$\begin{aligned} \overline{\langle D(E,t)\rangle} =& \overline{\langle Q(t)\rangle} \frac{\mu W_{\max}}{2(R_c^2 - R_{ex}^2/4)(E-E_0)} \\ & \times \int_{R_{ex}}^{2R_c} \exp\left(\frac{-2r}{R_D} - W_{\max} t e^{-2r/R_D}\right) \delta\left(r - \frac{ke^2}{\epsilon_1(E-E_0)}\right) r^2 dr. \end{aligned} \tag{4.8}$$

Using the sifting property of the Dirac delta function we evaluate the integral by replacing r with $ke^2/\epsilon_1(E-E_0)$ when $R_{ex} \leq ke^2/\epsilon_1(E-E_0) \leq 2R_c$. We also perform the change of variables $x = \frac{ke^2}{\epsilon_1 2R_c(E-E_0)}$, $\tau = W_{\max}t$, $\rho = R_c/R_D$, and $\epsilon = R_{ex}/2R_c$.

$$\overline{\langle D(x,\tau)\rangle} = \overline{\langle Q(t)\rangle} \frac{4\mu W_{\max} R_c \epsilon_1}{ke^2(1-\epsilon^2)} x^3 \exp\left(-4\rho x - \tau e^{-4\rho x}\right) H(x-\epsilon) H(1-x) \tag{4.9}$$

Note that these spectra are time resolved, meaning they represent the intensity of light emitted at each wavelength, at a particular time. To produce integrated spectra, one would need to numerically integrate Equations 4.7 and 4.9 with respect to time.

Comparing the red curves (with exclusion) to blue curves (without exclusion) we can see that the exclusion distance produces a hard cutoff at short wavelengths. This is expected since short wavelengths correspond to small donor-acceptor separations which are forbidden in this model. The short wavelength cutoff is higher in the 2D case because the exclusion distance is larger. Both curves also have a long wavelength cutoff due to the size of the nanocrystals. The maximum donor-acceptor separation is R_c in the 3D case and $2R_c$ in the 2D case.

Two issues are immediately obvious when comparing these plots to the experimental spectra in Figure 4.1. First, the peak occurs at a much shorter wavelength in the theoretical plots. Second, the theoretical spectra are much narrower, and in particular the cutoff range is very narrow. According to the data the cutoff range should be so wide that it does not show up in the spectrum. In the next section we will fix this second issue by deriving a correction to the photon energy due to the dielectric mismatch between the nanocrystals and the surrounding medium.

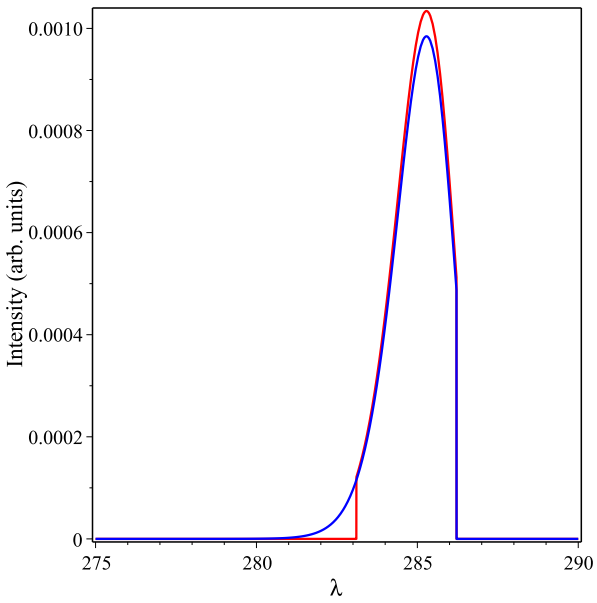

Figure 4.3: Spectrum for $R_c = 2.1$ nm crystals. 2D model at $t = 5$ μs with $E_0 = 4.3$ eV, $\epsilon_1 = 10.4$ and other parameters from Table 3.1. Blue curve has $R_{ex} = 0$

4.2 Dielectric Mismatch

The spectra above are narrower and centred at a lower wavelength than the experimental spectra. This is because Equation 4.1 for the energy of the emitted photons is a poor approximation. In this section we will develop a more accurate equation which takes into account the dielectric mismatch between the Ga_2O_3 nanocrystals and the surrounding medium. We will consider the modifications to the Coulomb interactions in a sphere in the presence of surface polarization charges due to a dielectric discontinuity at the surface.

We need to calculate the electric potential observed at point $\vec{r}$ due to a point charge q at point $\vec{r}_0$. The crystal has dielectric constant $\epsilon_1 = 10.6$ and the surrounding medium (hexane) has dielectric constant $\epsilon_2 = 1.88$. The problem is to solve Poisson's equation inside the crystal and Laplace's equation outside. The outer solution is not necessary for computing photon energies, but will be required for imposing boundary conditions. We follow the derivation given in Reference [24]. Using separation of variables, the potential

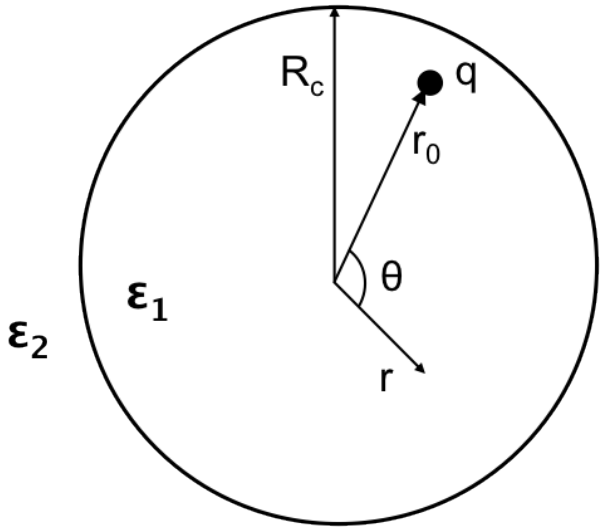

Figure 4.4: Observation point $\vec{r}$, Source point $\vec{r_0}$. Dielectric constants ϵ_1 inside, ϵ_2 outside.

inside, V_{in}, and outside V_{out}, can be written as

$$V_{in} = \frac{k}{\epsilon_1}\sum_{l=0}^{\infty}(A_l r^l + B_l r^{-l-1})P_l(\cos(\theta)) + V_c(\vec{r} - \vec{r_0}), \tag{4.10}$$

$$V_{out} = \frac{k}{\epsilon_2}\sum_{l=0}^{\infty}(C_l r^l + D_l r^{-l-1})P_l(\cos(\theta)), \tag{4.11}$$

where $A_l, B_l, C_l,$ andD_l are coefficients determined by the boundary conditions. The Coulomb term is $kq/\epsilon_1||\vec{r} - \vec{r_0}||$. It will be convenient later to write this in the form

$$V_c(\vec{r} - \vec{r_0}) = \frac{kq}{\epsilon_1}\sum_{l=0}^{\infty}\frac{r_<^l}{r_>^{l+1}}P_l(\cos(\theta)), \tag{4.12}$$

where $r_< = \min(r, r_0)$, $r_> = \max(r, r_0)$, and $P_l(x)$ is the l^{th} degree Legendre Polynomial which can be expressed, using Rodrigues' formula, as

$$P_l(x) = \frac{1}{2^l l!}\frac{d^l}{dx^l}[(x^2 - 1)^l]. \tag{4.13}$$

The following boundary conditions allow us to determine the coefficients $A_l, B_l, C_l,$ andD_l:

- V_{in} must remain bounded as $r \to 0$.
  This leads to $B_l = 0$.

- $V_{out} \to 0$ as $r \to \infty$.
  This leads to $C_l = 0$.

- $V_{in}(R_c) = V_{out}(R_c)$.
  This leads to $\frac{1}{\epsilon_1}(A_l R_c^l + q r_0^l R_c^{-l-1}) = \frac{1}{\epsilon_2} D_l R_c^{-l-1}$.

- $\epsilon_1 \frac{\partial V_{in}}{\partial r}(r = R_c) = \epsilon_2 \frac{\partial V_{out}}{\partial r}(r = R_c)$.
  This leads to $l A_l R_c^{l-1} - (l+1) q r_0^l R_c^{-l-2} = -(l+1) D_l R_c^{-l-2}$.

Solving the last 2 conditions for A_l and D_l gives

$$A_l = \frac{q_0 r_0^l (l+1)(\epsilon_1 - \epsilon_2)}{R_c^{2l+1}(l\epsilon_1 + (l+1)\epsilon_2)}, \tag{4.14}$$

$$D_l = \frac{q_0 r_0^l (2l+1)\epsilon_2}{l\epsilon_1 + (l+1)\epsilon_2} \tag{4.15}$$

Therefore the polarization term $(V_{in} - V_c)$ is

$$V_{pol}(\vec{r}, \vec{r_0}) = \frac{kq}{\epsilon_1 R_c}(\epsilon_1 - \epsilon_2) \sum_{l=0}^{\infty} \frac{l+1}{l\epsilon_1 + (l+1)\epsilon_2} \left(\frac{r r_0}{R_c^2}\right)^l P_l(\cos(\theta)) \tag{4.16}$$

The electrostatic self energy, or the image potential of a point charge q at $\vec{r_0}$ interacting with it's own image is given in terms of the polarization potential by

$$\begin{aligned} U_{im}(r_0) &= \frac{1}{2} q \lim_{\vec{r} \to \vec{r_0}} V_{pol}(\vec{r}, \vec{r_0}) \\ &= \frac{q^2}{2R_c\epsilon_1} \frac{\epsilon_1 - \epsilon_2}{\epsilon_1 + \epsilon_2} \left[\frac{1}{1 - (r_0/R_c)^2} + \frac{\epsilon_1}{\epsilon_1 + \epsilon_2} \Phi\left(\left(\frac{r_0}{R_c}\right), 1, \frac{\epsilon_2}{\epsilon_1 + \epsilon_2} \right) \right], \end{aligned} \tag{4.17}$$

where Φ is the Lerch Transcendent, defined as [25]

$$\Phi(z, s, a) = \sum_{k=0}^{\infty} \frac{z^k}{(a+k)^s}. \tag{4.18}$$

4.2.1 Initial State

The initial state, before recombination, has an electron with charge $q = -e < 0$ bound to a positively charged donor (at position $\vec{r}_D$), and neutral acceptor (at $\vec{r} = 0$). The main contribution to the energy of the system is the Coulomb interaction between the electron, at position $\vec{r}$, and the donor D^+, with charge $q = e > 0$. This gives the donor binding energy E_D. Perturbations to this state come from the interaction of the electron with the image of D^+ (given by $-eV_{pol}(\vec{r}, \vec{r}_D)$) and with it's own image ($U_{im}(\vec{r})$). Assuming that the electron is tightly bound to D^+ we can approximate it as having a hydrogenic wavefunction

$$\psi_D(\vec{r}) = C \exp\left(\frac{-||\vec{r} - \vec{r}_D||}{R_D}\right), \tag{4.19}$$

where R_D is the donor Bohr radius, and C is the non-radial part of the wavefunction. So the perturbation to the electron energy, E_D, in the initial state is

$$\begin{aligned} U_i &= \langle\psi_D| - eV_{pol}(\vec{r}, \vec{r}_D) + U_{im}(r) |\psi_D\rangle \\ &= \iiint |\psi_D|^2(-eV_{pol}(\vec{r}, \vec{r}_D) + U_{im}(r))d^3\vec{r}. \end{aligned} \tag{4.20}$$

Assuming that R_D is sufficiently small, $|\psi_D|^2 \to \delta(\vec{r} - \vec{r}_D)$. Evaluating this in the integral above gives

$$\begin{aligned} U_i &= -eV_{pol}(\vec{r}_D, \vec{r}_D) + U_{im}(r_D) \\ &= -U_{im}(r_D). \end{aligned} \tag{4.21}$$

4.2.2 Final State

The final state, after recombination, has an ionized donor D^+, and an electron bound to the neutral acceptor. This state has acceptor binding energy E_A, with perturbations from three sources. First is the coulomb interaction with D^+, $-eV_c(r_D)$. Second is the interaction with the image of the donor, $-eV_{pol}(0, r_D)$. Third is the interaction of the electron with it's own image, $U_{im}(0)$. The electron is now tightly bound to the acceptor so we approximate it as having a hydrogenic wavefunction,

$$\psi_A(\vec{r}) = C \exp\left(\frac{-||\vec{r}||}{R_A}\right), \tag{4.22}$$

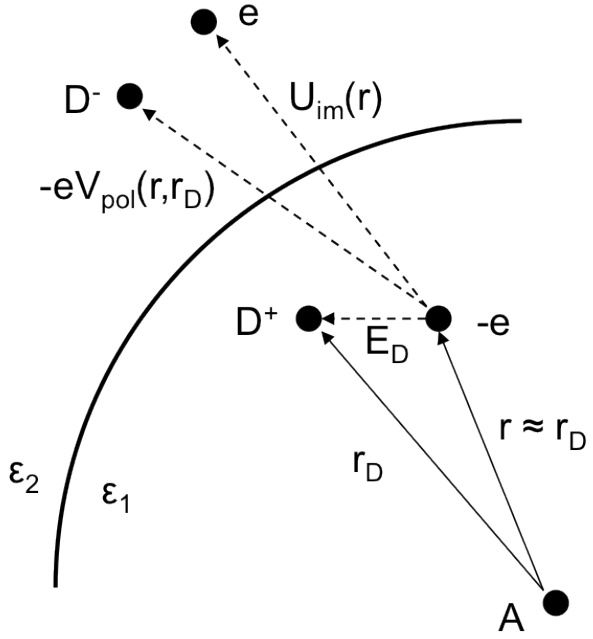

Figure 4.5: Initial state before recombination. The electron interacts with the positive donor (D^+), the negative image of the donor (D^-), and it's own positive image (e)

where R_A is the characteristic size of the elctron orbital in a potential well centered at the acceptor. So the perturbation to the acceptor binding energy, E_A, in the final state is

$$\begin{aligned} U_f &= \langle \psi_A | - eV_c(r_D) - eV_{pol}(\vec{r}, \vec{r}_D) + U_{im}(r) \, | \psi_A \rangle \\ &= \iiint |\psi_A|^2 (-eV_c(r_D) - eV_{pol}(\vec{r}, \vec{r}_D) + U_{im}(r)) d^3\vec{r}. \end{aligned} \tag{4.23}$$

We evaluate this as before assuming that $|\psi_A|^2 \to \delta(\vec{r})$.

$$\begin{aligned} U_f &= -eV_c(r_D) - eV_{pol}(0, r_D) + U_{im}(0) \\ &= -eV_c(r_D) - U_{im}(0). \end{aligned} \tag{4.24}$$

4.2.3 Energy Balance

The initial energy state is

$$E_i = E_D + U_i. \tag{4.25}$$

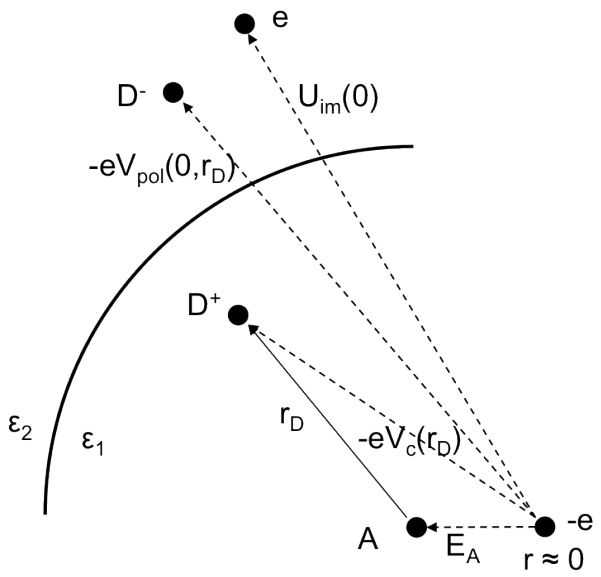

Figure 4.6: Final state before recombination. The electron interacts with the positive donor (D^+), the negative image of the donor (D^-), and it's own positive image (e)

The final energy state, after emitting a photon with energy hc/λ, is

$$E_f = \frac{hc}{\lambda} + E_A + U_f \tag{4.26}$$

Equating these and solving for the photon energy we get

$$\begin{aligned}\frac{hc}{\lambda} =& E_D - E_A + U_i - U_f \\ =& E_0 + \frac{ke^2}{\epsilon_1 r_D} + \frac{ke^2}{2R_c\epsilon_1}\left(\frac{\epsilon_1}{\epsilon_2} - 1\right) \\ & - \frac{ke^2}{2R_c\epsilon_1}\frac{\epsilon_1 - \epsilon_2}{\epsilon_1 + \epsilon_2}\left[\frac{1}{1-(r_D/R_c)^2} + \frac{\epsilon_1}{\epsilon_1+\epsilon_2}\Phi\left((r_D/R_c)^2, 1, \frac{\epsilon_2}{\epsilon_1+\epsilon_2}\right)\right].\end{aligned} \tag{4.27}$$

In deriving this correction to the photon energy we have made several limiting assumptions. First, we have placed the acceptor at the center of the nanocrystal, which means this is valid for the 3D model but not the 2D model. We have also assumed that the electron is tightly bound to the donor or acceptor, with a hydrogenic wavefunction. This lead us to approximate the electron wavefunction as a Dirac delta. This is a fairly crude assumption since the large values (> 1 nm) for the Bohr radius indicate that the wavefunction is not localized as a Dirac delta function.

Chapter 5

Monte Carlo Simulations

The models used so far have included many restrictions in order to evaluate them analytically. We have restricted our study to an acceptor located either in the center or on the surface of the nanocrystals and we have assumed that all crystals in a sample are the same size. Numerical methods are required in order to generalize this model. Here we describe a Monte Carlo method for generating an ensemble of nanocrystals and then evaluate the decay curve and spectrum that would be generated from that ensemble. Note that the words "sample" and "ensemble" are used interchangeably here and both refer to a collection of nanocrystals with properties drawn from the same distributions. For example all crystals in a sample will have the same radius, or each will have a radius drawn from the same distribution.

The Monte Carlo method is a numerical technique which involves generating random numbers. It is very useful for simulating large systems which contain uncertainty. The general idea is to generate random numbers in some domain, use these to perform some deterministic calculation, and then observe the results.

First we will describe the Monte Carlo algorithm for generating an ensemble of nanocrystal all with the same radius, with a single acceptor at the center, a fixed exclusion distance, a random number of donors drawn from a Poisson distribution, and donors uniformly distributed throughout the volume. We them make two generalizations: First we allow crystals in a sample to have different radii drawn from a normal distribution, and second we allow the acceptor to be randomly placed within the crystal.

5.1 Monte Carlo Algorithm

5.1.1 Generate Ensemble of Donor Distributions

We generate an ensemble of nanocrystal, each with a random number of donors distributed at random positions.

1. For each nanocrystal:
   (a) Generate random number of donors, n, from Poisson distribution. See Figure 5.1.
   (b) If $0 < n < n_{max}$ keep it. Otherwise discard it and re-draw. n_{max} is some large maximum number of donors (30 was chosen) included to simplify storage of donor position.
   (c) For each donor:
      i. Generate random numbers for donor position, $\{r, \theta, \phi\}$. Probability distribution for this is described in Section 5.2.
      ii. If $r < R_{ex}$ discard it and re-draw.

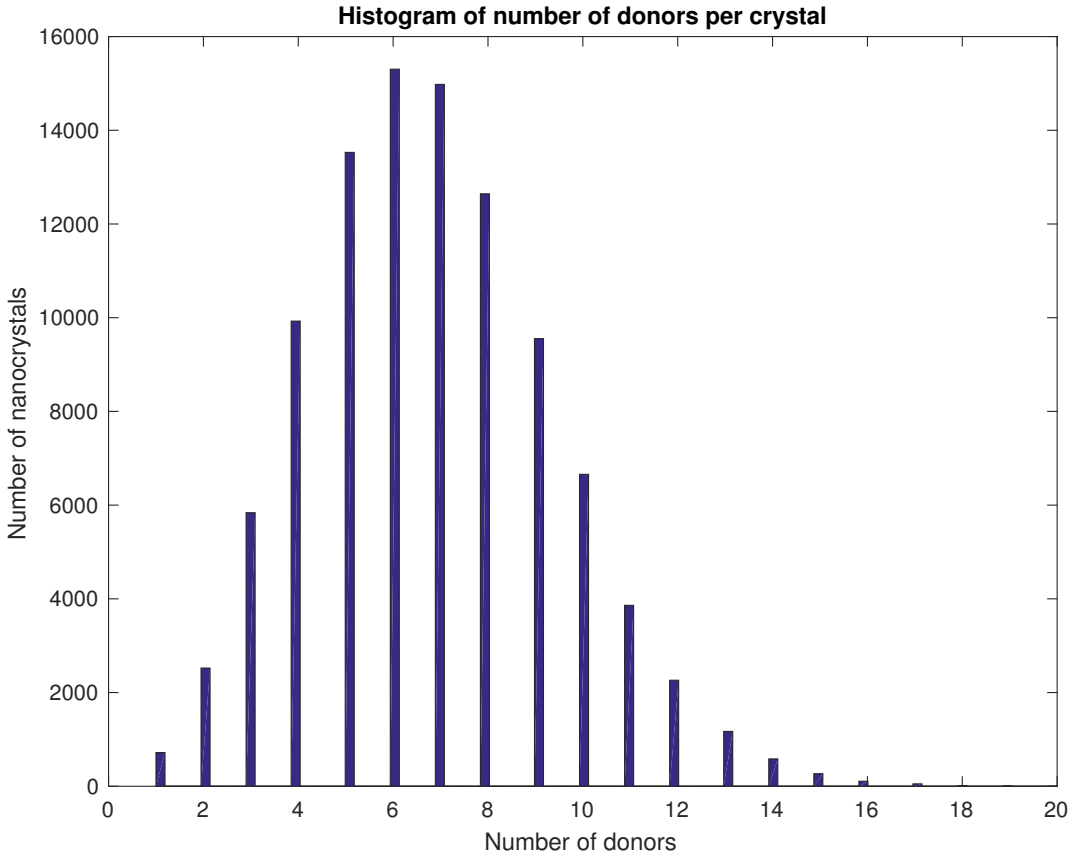

Figure 5.1: Simulated distribution of number of donors drawn from a Poisson distribution with average $\mu = 6.8$. The simulation contains a total of 100000 nanocrystals. Note that there are no crystals with zero donors in the simulation because these would not produce photoluminescence and are therefore unobservable.

Figure 5.2 shows a visualization of the nanocrystals generated by the Monte Carlo simulation. The red dot in the center is the acceptor and the blue dots are randomly distributed donors.

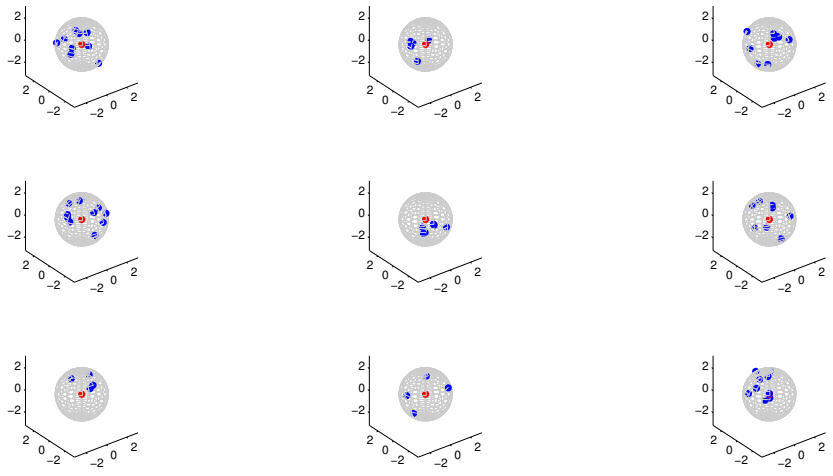

Figure 5.2: Ensemble of Monte Carlo nanocrystals with parameters from Table 3.1. Random number of donors (Poisson distribution with average $\mu = 6.8$) at random positions (uniformly distributed in the volume). 3D model with $R_c = 2.1$ and $R_{ex} = 0.92$. Red dots are acceptors, blue dots are donors. Units on the axes are nm.

5.1.2 Plot Decay Curve

We plot the intensity decay curve by averaging the decay rates of the donors over all nanocrystals.

1. For each nanocrystal:
   (a) Calculate decay rate of each donor using $W(r) = W_{\max} e^{-2r/R_D}$ and add this to the total decay rate for this crystal, $W_{\text{tot}} = \sum_{j=1}^{n} W(r_j)$ (i.e. the sum on the right hand side of Equation 2.5).
   (b) Decay curve for this crystal is given by $I(t) = W_{\text{tot}} e^{-W_{\text{tot}} t}$
2. Average decay curves at each time point. See Figure 5.3

Now we can use this algorithm to reproduce the experimental decay curves. Figure 5.3 shows simulated decay curves for three different sizes of nanocrystals. At early times the

simulation agrees very well with experiment. The curves are almost identical to those from the analytical model in Figure 3.2(a). At late times the fits are slightly worse than the ones from the analytical model in Figure 3.2(b). This may be due to the large acquisition time for the late time data. The analytical model handles this by using a finite difference (Equation 2.12) but the Monte Carlo simulation treats the intensity as an exact derivative.

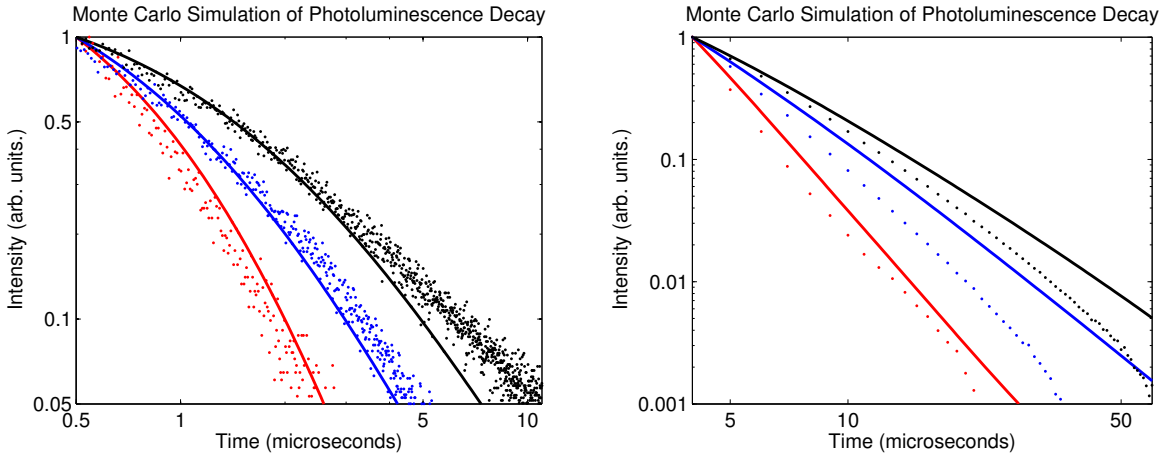

Figure 5.3: Solid lines are intensity decay curves generated using Monte Carlo simulation with parameters from Table 3.1. Dots are experimental data. $R_c = 1.55$ nm (red), 2.1 nm (blue), and 2.75 nm (black). Left shows early times, right shows late times.

5.1.3 Plot Integrated Spectrum

We plot the spectrum of emitted light by randomly choosing a donor from each nanocrystal to undergo recombination.

1. For each nanocrystal:
   (a) Choose a random number x uniformly distributed from 0 to 1.
   (b) For each donor:
      i. Add the decay rate for this donor to a counting decay rate for the whole crystal. $W_{count} = \sum_{j=1}^{k} W(r_j)$, where k refers to the current donor.
      ii. If $x \leq W_{count}/W_{tot}$ then this is the donor which recombines. Record the distance from this donor to the acceptor and exit the donor loop.

2. Use the list of donor-acceptor distances to generate a list of emitted photon wavelengths according to Equation 4.27

3. A histogram of these wavelengths represents the time integrated spectrum. See Figures 5.7 and 5.8.

5.2 Transformation of Probability Distributions

To choose random numbers for the position of the donors we need to transform from uniformly distributed random numbers, generated by Matlab, to other probability distributions. $f(x)dx$ gives the probability that a random variable x is in the interval $[x, x+dx]$. For two deterministically related random variables x and y the conservation of probability says that

$$f(x)dx = g(y)dy. \tag{5.1}$$

If x is uniformly distributed in the interval $[0, 1]$ then

$$f(x)dx = \left\{ \begin{array}{ccc} dx & , & 0 \leq x \leq 1 \\ 0 & , & \text{Otherwise} \end{array} \right\}. \tag{5.2}$$

Integrating both sides of Equation 5.1 we get.

$$x = \int_0^y g(y')dy' \tag{5.3}$$

Given a PDF $g(y)$ for the position of the donors, we integrate it and then invert to get $y(x)$. This is the function which will transform from a uniform distribution to $g(y)$. Here, the variable y stands for each coordinate r, θ, and ϕ, with a new independent x being generated for each coordinate.

5.2.1 Radial PDF

The probability of a donor being placed at a distance r is given by the surface area at that distance divided by the total volume of the crystal [26].

$$f(r) = \frac{4\pi r^2}{\frac{4}{3}\pi R_c^3}, \text{ for } 0 \leq r \leq R_c \tag{5.4}$$

Putting this into Equation 5.3 and integrating. we get

$$x = r^3/R_c^3. \tag{5.5}$$

Now we invert to get $r(x)$

$$r = R_c x^{1/3} \tag{5.6}$$

5.2.2 Polar Angle PDF

The PDF for the polar angle θ is [26]

$$f(\theta) = \frac{1}{2}\sin(\theta), \text{ for } 0 \leq \theta \leq \pi. \tag{5.7}$$

Integrating this we get

$$x = \frac{1}{2}(1 - \cos(\theta)), \tag{5.8}$$

and

$$\theta = \arccos(1 - 2x) \tag{5.9}$$

5.2.3 Azimuthal Angle PDF

The azimuthal angle ϕ is uniformly distributed on $[0, 2\pi]$ so the PDF is

$$f(\phi) = \frac{1}{2\pi}, \text{ for } 0 \leq \phi \leq 2\pi. \tag{5.10}$$

Integrating and inverting gives

$$\phi = 2\pi x \tag{5.11}$$

This inverse transform method can fail if the PDF cannot be integrated or inverted analytically. In that case a common technique is the Acceptance-Rejection method described in Appendix B.

5.3 Nanocrystal Size Distribution

Until now we have assumed that the crystal radius R_c is the same for all crystals in a sample. However, Figure 5.4 shows that the experimentally obtained crystal sizes are rather broadly distributed. To account for this in the Monte Carlo simulations we include a step where, for each nanocrystal, we generate a random crystal radius R_c from a normal distribution. The average crystal size and standard deviation are calculated from the histograms in Figure 5.4, and shown in Table 5.1. We must also restrict $R_c > R_{ex}$ for otherwise there would be nowhere to place the donors. See Figure 5.5 for a simulated crystal size distribution.

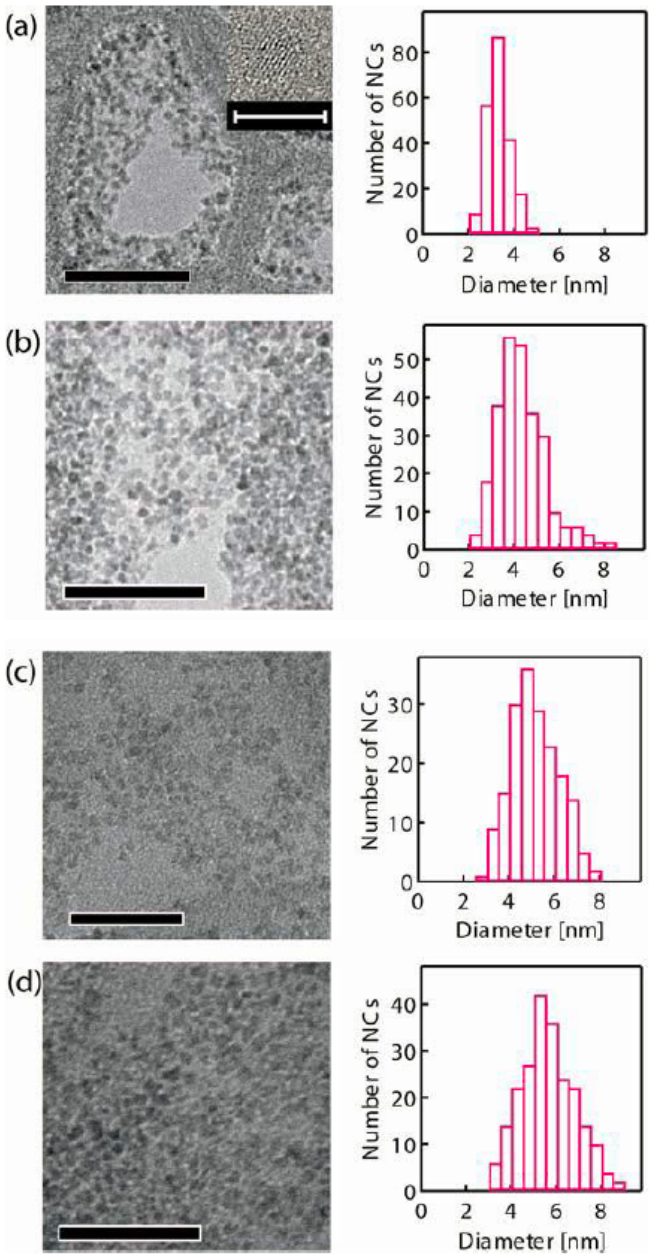

Figure 5.4: Transmission electron microscope images (left panels) and size distributions (right panels) of Ga_2O_3 nanocrystals. The size distributions were determined from the images by measuring about 200 nanocrystals. Scale bars in microscope images are 50 nm. The average nanocrystal diameters and standard deviations are: (a)3.3 $\pm$ 0.5, (b)4.2 $\pm$ 0.9, (c)5.1 $\pm$ 1.1, (d)5.5 $\pm$ 1.2 nm. Inset in (a) shows single nanocrystal (scale bar 5 nm). (Image from [17])

Average diameter (nm)	Standard deviation (nm)
3.3	0.5
4.2	0.9
5.1	1.1
5.5	1.2

Table 5.1: Observed nanocrystal size distribution. Measured from histograms in Figure 5.4

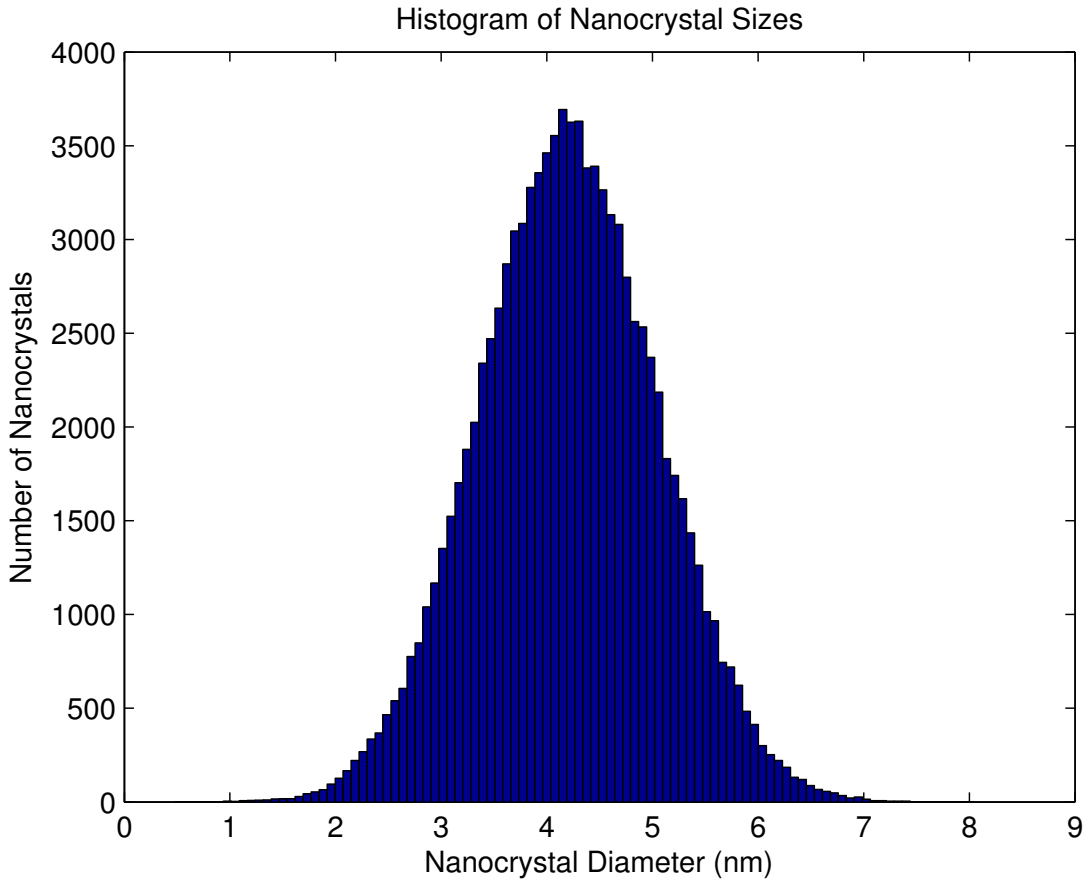

Figure 5.5: Simulated nanocrystal size distribution with average crystal diameter 4.2 ± 0.9 nm, drawn for a normal distribution. This corresponds to panel (b) in Figure 5.4

5.4 Arbitrary Acceptor Position

For the Monte Carlo simulations we have taken the acceptor to be at the center of the nanocrystal. This can be generalized by including a step in the algorithm where, for each crystal, we generate a random position for the acceptor using the distributions described in Section 5.2. See Figure 5.6 for a simulated ensemble of crystals with random acceptor positions. For the following spectra we will not use a random acceptor position because the dielectric modification was derived by assuming the acceptor was at the origin. This modification will need to be adjusted if we want to include random acceptor positions in our simulation.

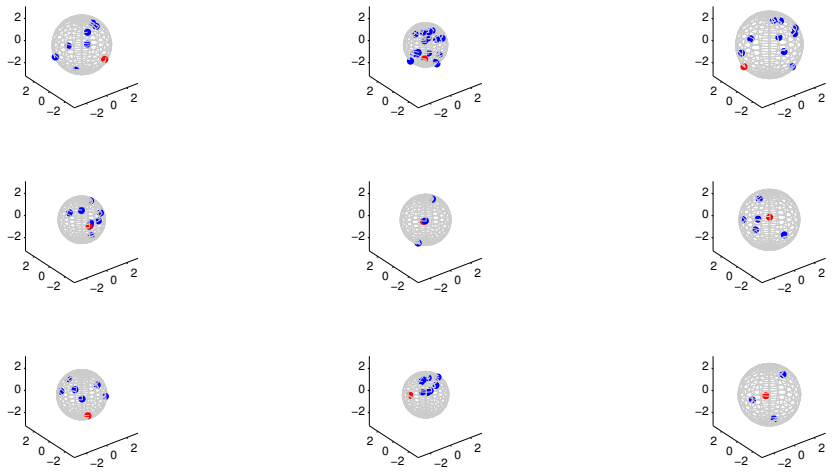

Figure 5.6: Ensemble of Monte Carlo nanocrystals with parameters from Table 3.1. Random number of donors (Poisson distribution with average $\mu = 6.8$) at random positions (uniformly distributed in the volume). Random crystal radius (normally distributed with average $R_c = 2.1$ nm and standard deviation 0.45 nm) and random acceptor position (uniformly distributed in the volume). Exclusion distance is $R_{ex} = 0.92$ nm, and units on the axes are nm.

5.5 Simulated Spectra

Here we simulate spectra using the best fit values in Table 3.1. Figure 5.7 shows the spectra with fitted exclusion value compared to no exclusion, and fixed crystal radius compared to distributed crystal radius. The exclusion distance produces a hard cutoff at short wavelengths as before. The effect of distributed crystal radius is very small. This is expected because looking at Figure 4.1 we see that the peak shift for different sizes of nanocrystals is only on the order of about 10 nm. However, for the case with exclusion distance the spectrum does become slightly broader, especially at shorter wavelengths, when distributed crystal radii are used.

One of the most obvious problems with the simulated spectra is the location of the peak. It is possible that the accepted values for the band gap energy, and donor and acceptor binding energies are only applicable for bulk Ga_2O_3, and may need to be modified for nanocrystals. Testing out several different values of the effective binding energy, it appears that $E_0 = 2.7$ gives the best agreements with experiment in terms of the locations of the spectral peak.

The second problem is the sharp cutoff at short wavelengths due to the exclusion distance, which does not appear in the experimental spectra in Figure 4.1. However we do see that the experimental spectrum is asymmetric, with a steep increase at short wavelengths and a long tail at long wavelengths. A possible solution for this is that instead of an exclusion distance with a sharp cutoff, we use some kind of ramp function. The spatial pdf for the donor positions would be an increasing function of the donor-acceptor separation. This would allow for donors to exist at short distances, removing the hard cutoff.

We can see in Figure 5.8 that the spectra are all peaked at 445 and 450 nm for the 2.1 and 2.75 nm crystals respectively. This agrees fairly well with the experimental data in Figure 4.1 which are peaked at 430 and 450 nm for the same size crystals. The fact that the peak wavelength increases with crystal size also agrees with the data. However it seems that the spectra become narrower as crystal radius increases which does not agree with the data. Despite this the Monte Carlo simulation seems very promising for exploring the effects of different assumptions and parameter choices in this model.

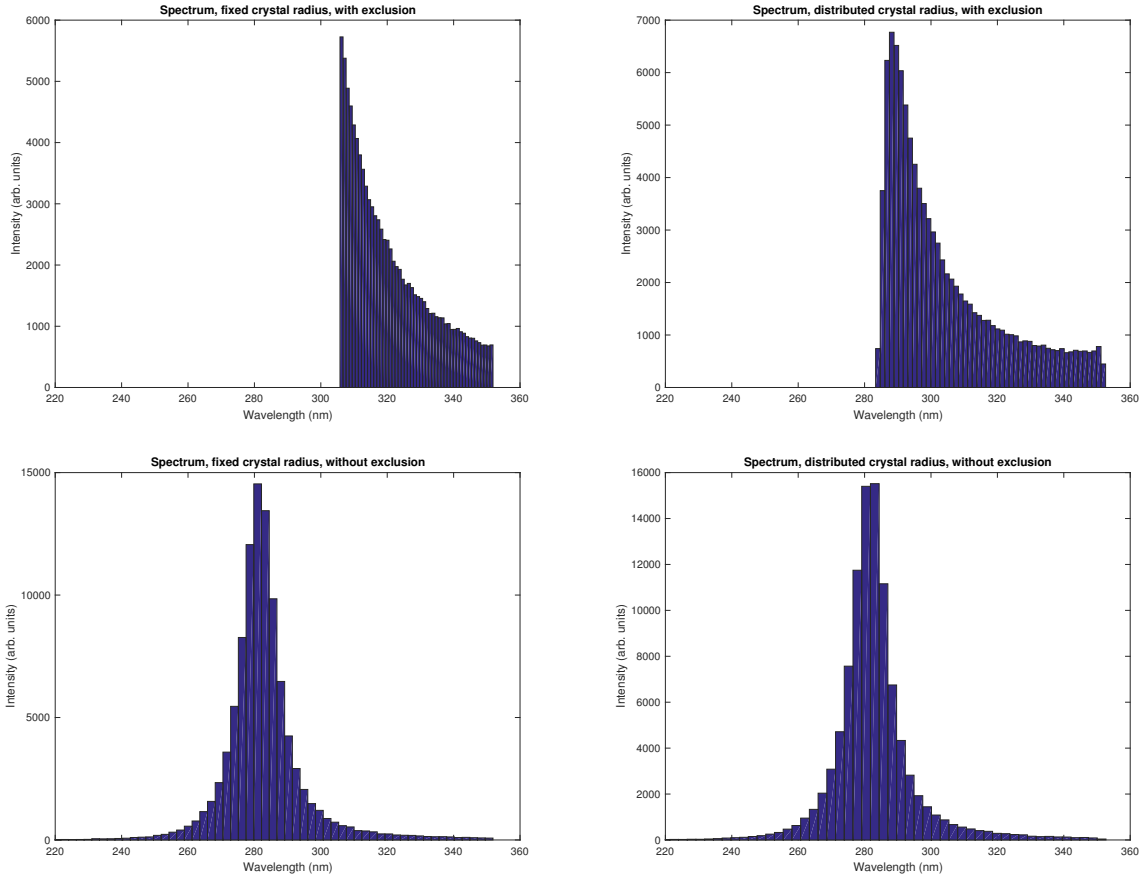

Figure 5.7: Spectra generated from best fit values in Table 3.1. $N_D = 6.6$, $R_D = 0.91$ nm, $E_0 = 4.3$ eV. Top has $R_{ex} = 1.5$ nm, bottom has $R_{ex} = 0$ nm. Left has fixed $R_c = 1.55$ nm, right has normally distributed R_c with average 1.55 nm and standard deviation 0.6 nm.

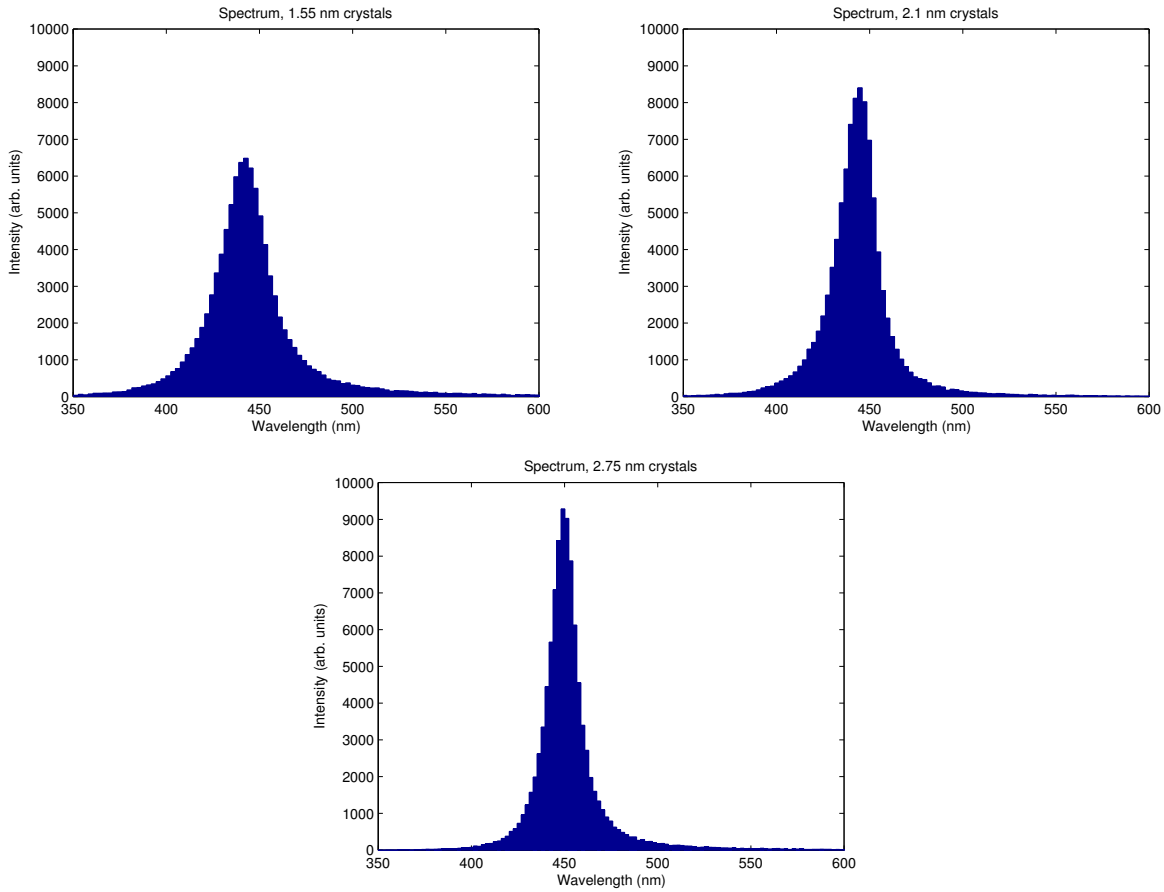

Figure 5.8: Spectra generated from best fit values in Table 3.1 for 3 sizes of crystals. $R_{ex} = 0$ nm, $E_0 = 2.7$ eV.

Chapter 6

Conclusion and Future work

6.1 Conclusions

We have developed a statistical model describing the photoluminescence decay dynamics in Ga_2O_3 nanocrystals. We explored several different cases for the distribution of donors and acceptors within the nanocrystals. A least squares procedure was used to fit the models to experimental data and a set of best fit parameters were obtained. We were able to fit both early and late time data very well with the same set of parameters. A model for the spectrum was developed which included the dielectric mismatch between the nanocrystals and their surroundings. A Monte Carlo algorithm was developed which produced ensembles of nanocrystals whose intensity decay and spectrum could be calculated. The intensity decay curves generated from the Monte Carlo simulation using the best fit parameters agree with experiment very well. However, the spectra from both the Monte Carlo simulation and the analytical model do not agree very well with experiment. They are peaked at much shorter wavelengths and have strong cutoffs at short wavelengths which are not observed in the data. The model can be generalized in a few ways.

We made the assumption that the donors are independent which allowed us to split the spatial probability distribution function into a product of first order probability distribution functions. This greatly simplified the calculation, however in reality donors do interact. This could be taken into account by including an exclusion distance around each donor as in Reference [26]. This would almost certainly make the equations unsolvable analytically, but it would be fairly simple to implement in the Monte Carlo simulation. When placing each donor one would need to check the distance to each of the other donors. If it is less

than the chosen exclusion distance it would be necessary to redraw a new random position for the donor.

The modification for a random donor position was described in Section 5.4, however it was not included in the simulations because the equation for the dielectric mismatch modification was derived with the assumption that the acceptor was at the origin. This modification could be rederived with an arbitrary acceptor position.

The spectrum models have not yet been fit to the data. Doing this will provide more information about the fitting parameters, especially the exclusion distance which is not yet fully understood. It is expected that the main role of the exclusion distance is a cut-off at short wavelengths which is not observed in the data.

With the recent advances in nanomaterials, and their substantial technological applications, it is becoming increasingly important to understand their properties and limitations. The photoluminescence properties of Ga_2O_3 are particularly promising for light emitting diodes and other optoelectronic devices, and studying the structural defects which affect these properties is key to unlocking their potential. On one hand this work has lead to a better understanding of defects in nanocrystals and their effect on photoluminescence, but it has also pointed to several issues in achieving a more complete model of defects and their interactions. As nanoctrustured materials become more common, especially in semiconductors, it is important to understand the formation and properties of defects.

Appendix A

Matlab Code for Monte Carlo Simulation

A.1 Main code

```
close all

W_max = 10^7; %max decay rate
R_c_avg = 1.55; %average nanocrystal radius
N_donors_avg = 6.6; %average number of donors
R_D = 0.91; %donor bohr radius

A_ex = 1.4; %acceptor exclusion radius
D_ex = 0; %donor exclusion radius

N_crystals = 10000; %Number of Nanocrystals
N_donors_max = 30; %max number of donors
t_start = -6; %start time power of 10
t_end = -4; %end time power of 10
time_points = 100; %number of time points

D_pos = zeros(N_crystals,N_donors_max,3); %vector of donor positions...
    %(r,theta,phi) theta azimuthal (0,pi), phi polar (0,2pi)
D_pos_cart = zeros(N_crystals,N_donors_max,3); %cartesian donor positions
```

```
A_pos = zeros(N_crystals,3); %vector of acceptor positions
A_pos_cart = zeros(N_crystals,3); %acceptor in cartesian
DA_dist = zeros(N_crystals,N_donors_max); %donor acceptor distances

N_donors = zeros(N_crystals,1); %number of donors in each crystal (random)
Crystal_sizes = zeros(N_crystals,1); %size of each crystal
W = zeros(N_crystals,1); %decay rates
Q = zeros(N_crystals,time_points); %decay function for each crystal
I = zeros(N_crystals,time_points); %intensity over time for each crystal

hc = 1240; %planks const * speed of light in electron volt nanometers
ke2 = 1.44; %e^2/4*pi*epsilon_0 in electron volt nanometers
dielec_gal = 10.6; %Relative dielectric constant of gallium oxide (10.6)
dielec_hex = 1.88; %Relative dielectric constant of Hexane solvent (1.88)
E_0 = 4.4; %E_gap-E_donor-E_acceptor in electron volts (4.9-0.2-0.3)
spec_dist = zeros(N_crystals,1); %Vector of distances for the donors...
    %that recombine


% 3D volume distribution: generate vector of donor positions
for crystal = 1:N_crystals

    %generate random size of crystal
    accept = false; %check crystal radius is between R_ex and 2*R_c_avg
    while accept == false
        R_c = normrnd(R_c_avg,0.2*R_c_avg);
        if R_c > A_ex && R_c < 2*R_c_avg
            accept = true;
        end
    end
    Crystal_sizes(crystal) = R_c;

    %generate random number of donors for each nanocrystal
    accept = false; %check if number of donors is less than max
    while accept == false
        N_donors(crystal) = poissrnd(N_donors_avg);
        if (N_donors(crystal) <= N_donors_max) && (N_donors(crystal) > 0)
            accept = true; %exits while loop
```

```
        end
    end

    %generate random acceptor position
    %A_pos(crystal,:) = [R_c*rand^(1/3), acos(1-2*rand), 2*pi*rand];
    [A_posX, A_posY, A_posZ] = sph2cart(A_pos(crystal,3),...
                                        pi/2-A_pos(crystal,2),...
                                        A_pos(crystal,1));
    A_pos_cart(crystal,:) = [A_posX,A_posY,A_posZ];


    for donor = 1:N_donors(crystal)
        accept = false; %Checks if donor position is accepted
        while accept == false

            %generate random position in spherical coordinates
            r = R_c*rand^(1/3);
            theta = acos(1-2*rand);
            phi = 2*pi*rand;

            %convert to cartesian to check distance
            [D_posX,D_posY,D_posZ] = sph2cart(phi, pi/2-theta, r);

            %check if donor is outside acceptor exclusion distance
            DA_dist(crystal,donor) = norm([D_posX,D_posY,D_posZ]...
                                          -[A_posX,A_posY,A_posZ]);
            if DA_dist(crystal,donor) > A_ex
                accept = true; %this will exit the while loop
                D_pos(crystal,donor,:) = [r, theta, phi]; %donor position
                D_pos_cart(crystal,donor,:) = [D_posX,D_posY,D_posZ];
            end
        end
    end
end
%%%%%%%%%%%%%%%%%%%%%%%%%%%%%%%%%%%%%%%%%%%%%%%%%%%%%%%%%%%%%%%%%%%%%%%%%%%%%%%
```

```
% 3D visualization
figure
hold on
[NC_X,NC_Y,NC_Z]=sphere; %sphere for nanocrystal
lightGrey = 0.8*[1 1 1]; %Make lines lighter on sphere

% plot donors and NC surface for each crystal
for crystal = 1:10
    subplot(2,5,crystal);

    %plot donors
    x=D_pos_cart(crystal,1:N_donors(crystal),1);
    y=D_pos_cart(crystal,1:N_donors(crystal),2);
    z=D_pos_cart(crystal,1:N_donors(crystal),3);
    scatter3(x,y,z,'filled');
    hold on
    scatter3(A_pos_cart(crystal,1),...
             A_pos_cart(crystal,2),...
             A_pos_cart(crystal,3),...
             'filled','MarkerFaceColor','r');

    %plot nanocrystal surface
    surface(Crystal_sizes(crystal)*NC_X,...
            Crystal_sizes(crystal)*NC_Y,...
            Crystal_sizes(crystal)*NC_Z,...
            'FaceColor', 'none','EdgeColor',lightGrey);
    %axis tight
    axis square
    axis([-1.5*R_c_avg 1.5*R_c_avg...
          -1.5*R_c_avg 1.5*R_c_avg...
          -1.5*R_c_avg 1.5*R_c_avg])
    %set(gca,'xtick',[],'ytick',[],'ztick',[])
    %grid off
    %axis off
end

%plot histogram of crystal sizes
```

```
figure
hist(Crystal_sizes,100)
title('Histogram of Nanocrystal Sizes');

%plot histogram of number of donors
figure
hist(N_donors,100)
title('Histogram of number of donors per crystal');
%%%%%%%%%%%%%%%%%%%%%%%%%%%%%%%%%%%%%%%%%%%%%%%%%%%%%%%%%%%%%%%%%%%%%%%%%%%%



% Decay rates
for crystal = 1:N_crystals
    for donor = 1:N_donors(crystal)
        r = DA_dist(crystal,donor);
        W(crystal) = W(crystal) + W_max*exp(-2*r/R_D);
    end
end
%%%%%%%%%%%%%%%%%%%%%%%%%%%%%%%%%%%%%%%%%%%%%%%%%%%%%%%%%%%%%%%%%%%%%%%%%%%%



% use decay rates to generate Intensity curves
Q_func = @(t) exp(-W.*t); %prob that acceptor is empty function
I_func = @(t) W.*exp(-W.*t); %intensity function
time = logspace(t_start,t_end,time_points); %generate logarithmically...
    %spaced time points for plotting
for t = 1:length(time)
    Q(:,t) = Q_func(time(t));
    I(:,t) = I_func(time(t));
end

%plot intensy for each nanocrystal
figure
for crystal = 1:N_crystals
    loglog(time,I(crystal,:));
    hold on
```

```
end

%average over all crystals (note: mean averages over first index)
I_avg = mean(I);

% plot intensity averaged over all crystals
figure
loglog(time,I_avg);
xlabel('Time (seconds)', 'fontsize',18);
ylabel('Intensity','fontsize',18);
title('Monte Carlo Simulation of Photoluminescence Decay','fontsize',18);
set(gca,'fontsize',18)

%plot histogram of radii
radii = zeros(sum(N_donors),1); %Vector for radii
count = 1;
%loop through crystals and donors, put r value in "radii"
for crystal = 1:N_crystals
    for donor = 1:N_donors(crystal)
        radii(count) = D_pos(crystal,donor,1);
        count = count + 1;
    end
end
figure
hist(radii,100)
title('Donor acceptor distances');
%%%%%%%%%%%%%%%%%%%%%%%%%%%%%%%%%%%%%%%%%%%%%%%%%%%%%%%%%%%%%%%%%%%%%%%%%%%%


% integrated spectrum
for crystal = 1:N_crystals
    W_count = 0; %hold sum of decay rates for looping through donors
    donor_picker = rand; %random number to pick which donor recombines
    for donor = 1:N_donors(crystal)
        r = DA_dist(crystal,donor);
        W_count = W_count + W_max*exp(-2*r/R_D);
        if donor_picker <= W_count/W(crystal) %check if this donor is...
```

```
                %the one that recombines
            spec_dist(crystal) = r; %save distance of recombined donor
            break %exit donor loop when one is chosen for recombination
        end
    end
end

%compute spectrum in energy and wavelength
spec_energies = E_0 + coulomb(ke2,dielec_gal,spec_dist) + dielec_mod(...
    ke2,dielec_gal,dielec_hex,Crystal_sizes,spec_dist); %Eneregy Spectrum
spec_wavelengths = hc./spec_energies; %Wavelength Spectrum

%plot histogram of distances of donors that recombine
figure
hist(spec_dist,100)
title('Distribution of Donor-Acceptor Recombination Distances');

%plot spectrum of energies
figure
hist(spec_energies,100)
title('Spectrum of Enegries of Emitted Photons');

%plot spectrum of wavelengths
figure
hist(spec_wavelengths,100)
title('Spectrum of Wavelengths of Emitted Photons');
%%%%%%%%%%%%%%%%%%%%%%%%%%%%%%%%%%%%%%%%%%%%%%%%%%%%%%%%%%%%%%%%%%%%%%%%%%%%%%%
```

A.2 Coulomb Function

```
function val = coulomb (ke2, dielec, r)

%Computes the Coulomb contribution to photon energy

val = (ke2/dielec)./r;
```

A.3 Dielectric Modification

```
function val = dielec_mod (ke2, dielec1, dielec2, R_c, r)

%Computes the modification to the Coulomb term due to dielectric mismatch

e1 = dielec1 / (dielec1 + dielec2);
e2 = dielec2 / (dielec1 + dielec2);

lerch_r = @(R) lerch(R, 1, e2);

Uim0 = coulomb(ke2,dielec1,2*R_c) * (e1/e2 - 1);

Uimr = coulomb(ke2,dielec1,2*R_c) .* (e1-e2) .* (1./(1-(r./(R_c+0.1)).^2)...
    + (e1) * arrayfun(lerch_r,(r./(R_c+0.1)).^2));

val = Uim0 - Uimr;
```

A.4 Lerch Function

```
function value = lerch ( z, s, a )

value = 0.0;

if ( z <= 0.0 )
  return
end

eps = 1.0e-10;
k = 0;
z_k = 1.0;

while ( 1 )

  if ( a + k ~= 0.0 )
    term = z_k / ( a + k )^s;
```

```
    value = value + term;

    if ( abs ( term ) <= eps * ( 1.0 + abs ( value ) ) )
      break
    end

  end

  k = k + 1;
  z_k = z_k * z;

end
```

Appendix B

Acceptance-Rejection Method

The inverse transform method above can fail if the PDF cannot be integrated or inverted. In this case we can use the following acceptance-rejection method [27]. Suppose we have a target PDF $f(x)$ which is restricted to the interval $[a, b]$. Let $c \geq \max f(x) : x \in [a, b]$. The following algorithm generates a random variable Y with the desired PDF:

1. Generate X uniform in $[a, b]$.
2. Generate Y uniform in $[0, c]$ independently of X.
3. If $Y \leq f(X)$ accept Y, otherwise reject it.

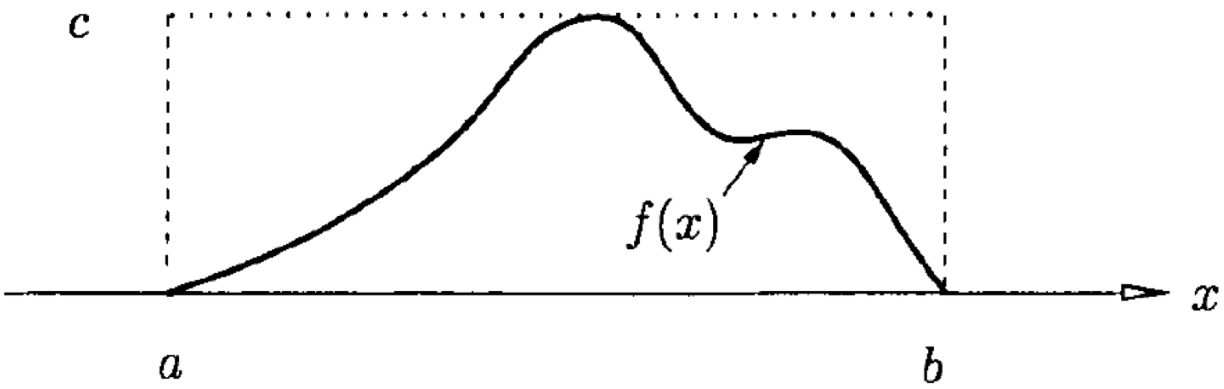

Figure B.1: Acceptance-rejection method (Image from [27])

This method contains some amount of "wasted" space because all value of Y above $f(X)$ are rejected. We can minimize this waste in the following way. Choose a proposal distribution $g(x)$ such that $g(x) \geq f(x)$ for all $x \in [a, b]$. The PDF $g(x)$ should be one that it is easy to generate random variables from. The generalized acceptance-rejection algorithm is:

1. Generate X from g(x).
2. Generate Y uniformly in $[0, g(X)]$.
3. If $Y \leq f(X)$ accept Y, otherwise reject it.

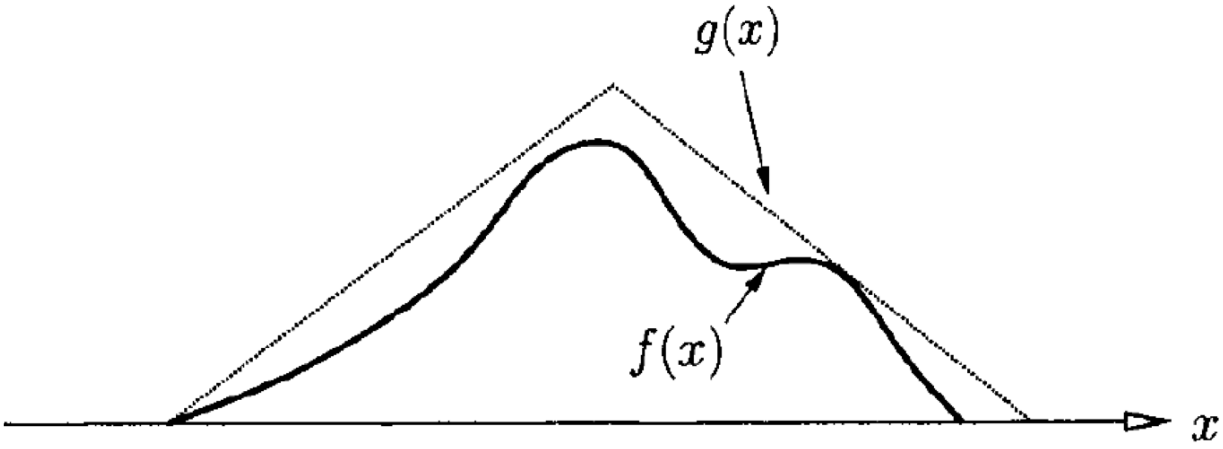

Figure B.2: Generalized acceptance-rejection method with proposal distribution $g(x)$ (Image from [27])

Choosing a proposal distribution $g(x)$ which is close to $f(x)$ will minimize the wasted draws. However higher dimensions will usually have more wasted space. For example a circle inscribed in a square takes up $\pi/4 \approx 0.79$ of the area, but a sphere inscribed in a cube takes up only $\pi/3 \approx 0.52$ of the volume.

Appendix C

Derivation of Decay Rate

Here we calculate the decay rate given in Equation 1.2. This derivation follows Reference [28]. The decay rate is the probability per unit time for the system to transition from an initial state, with the electron on a donor, to a final state, with the electron on the acceptor. The electromagnetic field and therefore the Hamiltonian for this process is time dependent so we must use time dependent perturbation theory.

The full Hamiltonian can be written as $H = H_0 + H_{int}(t)$, where H_0 is the time-independent part, and $H_{int}(t)$ is the time-dependent interaction part. It is convenient to expand the full time-dependent wavefunction as $\Psi(\mathbf{r},t) = \sum_k c_k(t)\psi_k(\mathbf{r})\exp(-iE_kt/\hbar)$, where the $\psi_k(\mathbf{r})$ are the eigenfunctions of H_0, and the $c_k(t) = c_k^0(t) + c_k^1(t) + \ldots$ are the time-dependent expansion coefficients to be computed using perturbation theory. The zero-order approximation is $c_k^0(t) = \delta_{ki}$ since only the initial state i is occupied at time $t = 0$. The first order approximation is then given by [28]

$$c_j^1(t) = \frac{1}{i\hbar}\int_0^t \langle\psi_j|\, H_{int}(t')\,|\psi_i\rangle \exp[i(E_j - E_i)t'/\hbar]dt' \tag{C.1}$$

Now we consider a time-dependent interaction Hamiltonian of the form

$$H_{int}(t) = h(\mathbf{r})e^{-i\omega t} + h^\dagger(\mathbf{r})e^{i\omega t}, \tag{C.2}$$

where, for an electron in a plane electromagnetic field,

$$h(\mathbf{r}) = \frac{e}{m_e c}\left\{\mathbf{A}_0 e^{i\mathbf{k}\cdot\mathbf{r}}\cdot\mathbf{p} + \frac{\hbar}{2}\boldsymbol{\sigma}\cdot[i\mathbf{k}\times\mathbf{A}_0 e^{i\mathbf{k}\cdot\mathbf{r}}]\right\}. \tag{C.3}$$

Here $\mathbf{A}_0$ is the strength of the magnetic vector potential, $\mathbf{k}$ is the wavevector of electromagnetic radiation, $\mathbf{p}$ is the momentum operator of an electron undergoing transition, and $\boldsymbol{\sigma}$ is the electron spin operator.

We now substitute $H_{int}(t)$ into Equation C.1 and perform the integration over t'. The resulting expression contains two terms. For large t the first term is important only when $E_j - E_i - \hbar\omega \approx 0$, which corresponds to absorption. Similarly the second term is important only when $E_j - E_i + \hbar\omega \approx 0$, which corresponds to emission. In our case we are interested in emission, so the probability that the system jumps from state i to state j is given to first order by

$$|c_{ji}^1(t)|^2 = \frac{1}{\hbar^2} |\langle\psi_j| h^\dagger |\psi_i\rangle|^2 \left\{ \frac{\sin[(E_j - E_i + \hbar\omega)t/2\hbar]}{(E_j - E_i + \hbar\omega)/2\hbar} \right\}^2. \tag{C.4}$$

As a function of ω the term in brackets is sharply peaked at $(E_i - E_j)/\hbar$, and the square of this term is well approximated by $2\pi t\hbar$ times a delta function. Dividing by t we get the the transition rate for emission at frequency ω is

$$\frac{|c_{ji}^1(t)|^2}{t} = \frac{2\pi}{\hbar} |\langle\psi_j| h^\dagger |\psi_i\rangle|^2 \delta(E_j - E_i + \hbar\omega). \tag{C.5}$$

Next we need to calculate the transition probability for emitting a photon at frequency ω into a solid angle element $d\Omega$ about the wavevector $\mathbf{k}$. This requires the density of states per unit energy per unit solid angle which is give by [28]

$$\frac{d^3\rho(E = \hbar\omega)}{dE d\Omega} = \frac{V\omega^2}{\hbar(2\pi c)^3}, \tag{C.6}$$

where V is the volume in which the radiation field exists. Then the transition rate per unit time per unit solid angle is given by

$$\frac{dW}{d\Omega} = \int \frac{|c_{ji}^1|^2}{t} \frac{d^3\rho(E = \hbar\omega)}{dE d\Omega} d(\hbar\omega) \tag{C.7}$$

$$\propto |\langle\psi_j| e^{-i\mathbf{k}\cdot\mathbf{r}} \mathbf{p} |\psi_i\rangle \cdot \mathbf{e}^{(\alpha)}|^2 \tag{C.8}$$

where α represents the two polarization states of the radiation and $e^{-i\mathbf{k}\cdot\mathbf{r}}\mathbf{p}$ is the first term from $h^\dagger$. Since the wavelength of the emitted photon is much larger than the size of the atom $|\mathbf{k}||\mathbf{r}| << 1$, so $e^{-i\mathbf{k}\cdot\mathbf{r}} \approx 1$.

To compute the matrix element $\langle\psi_j| \mathbf{p} |\psi_i\rangle$ we assume that the initial and final states have Hydrogenic wavefunctions of the form $e^{-a||\mathbf{r}||}$, and that the acceptor has a higher

binding energy than the donor, which allows us to approximate the acceptor wavefunction as a Dirac delta. Then the matrix element becomes

$$\begin{aligned}\langle\psi_j|\,\mathbf{p}\,|\psi_i\rangle &= \int \psi_A(\mathbf{r}'-\mathbf{r})\mathbf{p}\psi_D(\mathbf{r}')d^3\mathbf{r}' \\ &\propto \psi_D(r) \\ &\propto e^{-r/R_D}.\end{aligned}$$

Finally, we integrate over solid angle and sum over the polarization states to obtain the decay rate,

$$W(r) = W_{\max}e^{-2r/R_D} \tag{C.9}$$

where constants are combined into $W_{\max}$, and R_D is the donor Bohr radius.

References

[1] M. Achermann, M. A. Petruska, S. Kos, D. L. Smith, D. D. Koleske, and V. I. Klimov. *Nature*, 429:642, 2004.

[2] D. V. Talapin and C. B. Murray. *Science*, 310:86, 2005.

[3] J. B. Sambur, T. Novet, and B. A. Parkinson. *Science*, 330:63, 2010.

[4] Z. Li, C. de Groot, and J. H. Moodera. *Appl. Phys. Lett.*, 77:3630, 2000.

[5] M. Passlack, N. E. J. Hunt, E. F. Schubert, G. J. Zydzik, M. Hong, J. P. Mannaerts, R. L. Opila, and R. J. Fischer. *Appl. Phys. Lett.*, 64:2715, 1994.

[6] A. M. Stoneham. *Theory of Defects in Solids: Electronic Structure of Defects in Insulators and Semiconductors*. Claredon, 1975.

[7] P. J. Dean. *Progress in Solid State Chemistry*, 8:1–126, 1973.

[8] C. C. Chen, A. B. Herhold, C. S. Johnson, and A. P. Alivisatos. *Science*, 276:398, 1997.

[9] R. Beaulac, S. T. Ochsenbein, and D. R. Gamelin. *Nanocrystal Quantum Dots*, page 397, 2010.

[10] C. Janowitz et al. *New J. Phys.*, 13:085014, 2011.

[11] Solid-state lighting research and development portfolio: Multi-year program plan fy'07-fy'12, navigant consulting, inc., 2007, prepared for lighting research and development building technologies program, office of energy efficiency and renewable energy, u.s. dept. of energy.

[12] Wan Hang Melanie Chiu. Förster resonance energy transfer mediated white-light-emitting rhodamine fluorophore derivatives-gamma phase gallium oxide nanostructures. Master's thesis, University of Waterloo, 2012.

[13] T. Wang, S. S. Farvid, M. Abulikemu, and P. V. Radovanovic. *J. Am. Chem. Soc.*, 132:9250–9252, 2010.

[14] M. Hedge, T. Wang, Z. L. Miskovic, and P. V. Radovanovic. *Appl. Phys. Lett.*, 100:141903, 2012.

[15] A. Blumen, J. Klafter, and G. Zumofen. *J. Chem. Phys.*, 84:1397 – 1401, 1986.

[16] J. Klafter and A. Blumen. *Journal of Luminescence*, 34:77 – 82, 1985.

[17] Ting Wang. *Investigation of the Optical Properties of Nanostructured Transparent Conducting Oxides*. PhD thesis, University of Waterloo, 2013.

[18] C. R. Ronda. *Luminescence From Theory to Applications*. Wiley, 2008.

[19] J. R. Lakowicz. *Principles of Fluorescence Spectroscopy*. Springer, 3^{rd} edition, 2006.

[20] T. Wang and P. V. Radovanovic. *J. Phys. Chem. C*, 115:18473, 2011.

[21] L. Binet and D. Gourier. *J. Phys. Chem. Solids*, 59:1241, 1998.

[22] D. G. Thomas, J. J. Hopfield, and W. M. Augustyniak. *Phys. Rev.*, 140:A202, 1965.

[23] D. Fu and T. W. Kang. *Jpn. J. Appl. Phys.*, 41:L1437, 2002.

[24] T. P. Doerr and Yi-Kou Yu. *Am. J. Phys.*, 72:190, 2004.

[25] F. W. J. Olver, D. W. Lozier, R. F. Boisvert, and C. W. Clark, editors. *NIST Handbook of Mathematical Functions*. Cambridge University Press, New York, NY, 2010.

[26] S. F. Swallen, K. Weidemaier, and M. D. Fayer. *J. Phys. Chem.*, 99:1856, 1995.

[27] R. Rubinstein and D. Kroese. *Simulations and the Monte Carlo Method*. Wiley, 2008.

[28] Y. B. Band. *Light and Matter: Electromagnetism, Optics, Spectroscopy and Lasers*. Wiley, 2006.

[29] R. F. Khairutdinov and N. Serpone. *Prog. Reaction Kinetics*, 21:1–68, 1996.

[30] T. Wang, V. Chirmanov, W. H. M. Chiu, and P. Radovanovic. *J. Am. Chem. Soc.*, 135:14520–14523, 2013.

[31] C. Kittel. *Introduction to Solid State Physics*. John Wiley & Sons, 8^{th} edition, 2005.

[32] V. Malkov. Theoretical modelling of photoluminescence decay dynamics in $\gamma - ga_2o_3$ nano-crystals. Technical report, University of Waterloo, 2013.

[33] H. H. Tippins. *Phys. Rev.*, 140:A316, 1965.

[34] K. Takahashi, A. Yoshikawa, and A. Sandhu. *Wide Bandgap Semiconductors*. Springer, 2007.

[35] Raphael Tsu, Davorin Babic, and Liderio Ioriatti Jr. *J. Appl. Phys*, 82:1327, 1997.

[36] K. U. Finger, A. H. Marcus, and M. D. Fayer. *J. Chem. Phys.*, 100:271, 1994.

[37] R. Tsu and D. Babic. *Appl. Phys. Lett.*, 64:1806, 1994.

[38] E. C. Niculescu. *Optics Communications*, 284:3298, 2011.

[39] G. J. Yi and G. F. Neumark. *Phys. Rev. B*, 48:17043, 1993.

[40] P. T. Landsberg and M. J. Adams. *Proc. R. Soc. Lond. A*, 334:523, 1973.

[41] V. Novotny. *Can. J. Phys.*, 47:1971, 1969.

[42] C. Robert and G. Casella. *Monte Carlo Statistical Methods*. Springer, 2008.

[43] S. I. Stepanov, V. I. Nikolaev, V. E. Bougrov, and A. E. Romanov. *Rev. Adv. Mater. Sci.*, 44:63, 2016.